

We thank the referees for their reviews. To facilitate the review process we have copied the reviewer comments in black text. Our responses are in regular blue font. We have responded to all the referee comments and made alterations to our paper (**in bold text**). Figures, tables, and sections in the responses are numbered as in the *revised* manuscript unless specified, while page and line numbers refer to the ACPD paper.

Anonymous Referee #1

In the study at hand, a previously developed kinetic box model is applied to a plethora of scenarios that could be encountered when using oxidation flow reactors (OFR) to produce secondary organic aerosol (SOA) in the presence of NO. Peng et al. present a very detailed study that, while not directly relevant for the general public, might be very helpful for the specialized field of atmospheric researchers employing OFR and falls within the scope of ACP. Especially the comprehensive Fig. S7 should be a fantastic resource for research groups working with OFR and without excess to kinetic modelling tools. The authors convincingly show that the conditions in which OFR are often operated are far from atmospheric relevance.

R1.0) The article is well-structured, but is now and then difficult to read, e.g. in Sects. 3.1.1 and 3.2. A reason for this might be that the narrative doesn't closely follow the figures, and, while the figures contain lots of useful information, it seems that much of the given information is not discussed in the manuscript, which would technically render most of the figures in the main text supplementary material. I would like to encourage the authors at this point to re-think their use of figures in this manuscript. For example, can the information in Figure 1 be presented in a more concise, meaningful way? It also does not help that positions and sizes of fonts and symbols in Fig. 1 are different in all three panels. This does not diminish the solid scientific message of this work, but would help immensely to reach a larger audience. Thus, I can recommend this paper for publication in ACP after only minor revisions, but would encourage the authors to revise the visual presentation of their scientific results. Further point-by-point comments are given below.

We have made the sizes of fonts and symbols identical in the 3 panels of Fig. 1. To improve the legibility of Sections 3.1.1 and 3.2, we have made modifications to the text in a number of places: reformulating/reordering sentences, adding/improving references to figures, clarifying some details etc. In particular, we have referred to Fig. S7 in the ACPD version (Fig. S3 in the revised version; other figures in SI also renumbered accordingly) in these sections as well as elsewhere in the paper to better take advantage of its large amount of useful information. Note that Fig. S7 (in the ACPD version) was included mainly for experimental planning purposes. We did not aim to explain every feature in Fig. S7 in the ACPD version and have only referred to it when useful, and have not substantially changed the text just according to the material in this figure.

The modified Sections 3.1.1 and 3.2 now read as follows:

Section 3.1:

“In OFR185-iNO, NO is *not* oxidized extremely quickly under *all* conditions. For instance, under a typical condition in the midrange of the phase space shown in Fig. 1a, $t_{NO} \sim 13$ s. This lifetime is much shorter than the residence time, but long enough for OH_{exp} to reach $\sim 3 \times 10^{10}$ molecules cm^{-3} s, which is equivalent to an OH equivalent age of ~ 6 hrs. Such an OH equivalent age is already sufficient to allow some VOC processing and even SOA formation to occur (Lambe et al., 2011; Ortega et al., 2016). Within t_{NO} , NO suppresses HO_2 through the reaction $NO + HO_2 \rightarrow NO_2 + OH$, leading to NO_{exp}/HO_{2exp} of ~ 700 during this period, high enough for RO_2 to dominantly react with NO. Meanwhile, $NO + HO_2 \rightarrow NO_2 + OH$ enhances OH production, which helps OH_{exp} build up in a relatively short period. In addition, non-tropospheric photolysis of VOCs at 185 and 254 nm is minor ($F_{185exp}/OH_{exp} \sim 600$ cm/s, Fig. 1a), because of enhanced OH production and moderate UV. Therefore, such an OFR condition may be of some interest for high-NO VOC oxidation. We thus analyze the NO_y chemistry in OFR185-iNO in more detail below, by taking the case shown in Fig. 1a as a representative example.

In OFR185-iNO, HO_x concentrations are orders-of-magnitude higher than in the atmosphere while the amount of O_3 produced is relatively small during the first several seconds after the flow enters the reactor. As a result, NO is not oxidized almost exclusively by O_3 as in the troposphere, but also by OH and HO_2 to form HONO and NO_2 , respectively (Fig. 1a). The large concentration of OH present then oxidizes HONO to NO_2 , and NO_2 to HNO_3 . Photolysis only plays a negligible role in the fate of HONO and NO_2 in OFRs, in contrast to the troposphere, where it is the main fate of these species. This is because the reactions of HONO and NO_2 with OH are greatly accelerated in OFR compared to those in the troposphere, while photolysis not (Peng et al., 2016). The interconversion between NO_2 and HO_2NO_2 is also greatly accelerated (Fig. 1a), since a large amount of HO_2 promotes the formation of HO_2NO_2 , whose thermal decomposition and reaction with OH in turn enhance the recycling of NO_2 . Though not explicitly modeled in this study, RO_2 are expected to undergo similar reactions with NO_2 to form reservoir species, i.e., peroxy nitrates (Orlando and Tyndall, 2012). Peroxy nitrates that decompose on timescales considerably longer than OFR residence times may serve as effectively permanent NO_y sinks in OFRs (see Section 3.4.1).

Interestingly but not surprisingly, the NO_y chemistry shown in Fig. 1a is far from temporally uniform during the OFR residence time (Fig. S1a). Within t_{NO} , NO undergoes an e-fold decay as it is rapidly converted into NO_2 and HONO, whose concentrations reach maxima around that time. After most NO is consumed, HONO and NO_2 also start to decrease, but significantly more slowly than NO, since they do not have as many and efficient loss pathways as NO. The reaction of OH with HONO, the dominant fate of HONO, is slower than that with NO (Fig. 1a). The net rate of the NO_2 -to- HO_2NO_2 conversion becomes low because of the relatively fast reverse reaction (Fig. 1a). Besides, the total loss of NO_2 is partially offset by the production from HONO. The generally stable concentrations of HONO and NO_2 (Fig. S1a) result in their respective reaction rates with OH that are comparable during and after t_{NO} (Fig. 1a), as OH variation is also relatively small during the

entire residence time (Fig. S1b). However, the NO_2 -to- HO_2NO_2 conversion after τ_{NO} is much faster than during it (Fig. 1a), resulting from substantially decreased NO and HO_2 concomitantly increasing >1 order of magnitude after τ_{NO} (Fig. S1a,b). HNO_3 and HO_2NO_2 , which are substantially produced only after NO_2 is built up, have much higher concentrations later than within τ_{NO} .

Under other OFR185-iNO conditions than in Fig. 1a, the major reactions interconverting NO_y species are generally the same, although their relative importance may vary. At lower NO^{in} , the perturbation of HO_x chemistry caused by NO_y species is smaller. Effects of NO^{in} less than 1 ppb (e.g., typical non-urban ambient concentrations) are generally negligible regarding HO_x chemistry. Regarding NO_y species, the pathways in Fig. 1a are still important under those conditions. At higher NO^{in} (e.g., >1 ppm), one might expect NO_3 and N_2O_5 to play a role (as in OFR254-iNO; see Section 3.1.2 below), since high NO_y concentrations might enhance self/cross reactions of NO_y . However, this would not occur unless OH production is high, since relatively low O_3 concentrations in OFR185-iNO cannot oxidize NO_2 to NO_3 rapidly. Also, a large amount of NO_y can lead to significant OH suppression. That would in turn slow down the NO_3 production from HNO_3 by OH. This is especially true when an OFR is used to oxidize the output of highly concentrated sources (e.g., from vehicle exhausts). When sources corresponding to OHR_{ext} of thousands of s^{-1} and NO^{in} of tens of ppm are injected into OFR185 (Fig. 1b), they essentially inhibit active chemistry except NO consumption, as all subsequent products are much less abundant compared to remaining NO (Fig. S1c)."

And Section 3.2:

"Having illustrated the main NO_y chemical pathways for typical cases, we present the results of the exploration of the entire physical parameter space (see Section 2.2). Note that the explored space is indeed very large and gridded logarithmically uniformly in every dimension. Therefore, the statistics of the exploration results can be useful to determine the relative importance of the conditions types defined in Section 2.2 and Table 3.

It has been shown that during τ_{NO} , RO_2 can react dominantly with NO (Section 3.1.1), while to determine if a condition is high-NO (see Table 3), the entire residence time is considered. This is done because for VOC oxidation systems of interest, there will be significant oxidation of the initial VOC and its products under low-NO conditions, if τ_{NO} is shorter than the reactor residence time. After most NO is consumed, the longer the remaining residence time, the more RO_2 will react with HO_2 and the more likely that an input condition is classified as low-NO. For a condition to be high-NO, a significantly long τ_{NO} is required. Figure 3 shows the fractional occurrence distribution of good/risky/bad conditions in the entire explored condition space over logarithm of $r(\text{RO}_2+\text{NO})/r(\text{RO}_2+\text{HO}_2)$, which distinguishes high- and low-NO conditions. In OFR254-iNO, τ_{NO} is so short that no good high-NO condition is found in the explored range in this study (Fig. 3a). A fraction of explored conditions are bad high-NO. These conditions result from a full consumption of O_3 by NO. Then very little HO_x is produced (right panels in Fig. S3h), but the fate of any RO_2 formed is dominated by RO_2+NO (right panels in Fig. S3i). However, also due to

negligibly low OH concentration, little RO₂ is produced and non-tropospheric photolysis of VOCs is also substantial compared to their reaction with OH under these conditions, classifying all of them as “bad” (Fig. 3a).

In OFR185-iNO, in addition to the typical case shown in Fig. 1a, many other cases have a τ_{NO} of ~10 s or longer (Figs. S3b and S4), which allow the possibility of high-NO conditions. Indeed, ~1/3 of explored conditions in OFR185-iNO with a residence time of 3 min are high-NO (Fig. 3b). Most of these high-NO conditions are also classified as bad, similar with those in OFR254-iNO. More importantly, in contrast to OFR254-iNO, good and risky high-NO conditions also comprise an appreciable fraction of the OFR185-iNO conditions. It is easily expected that very high OHR_{ext} and NOⁱⁿ lead to bad high-NO conditions (all panels in Fig. 4), since they strongly suppress HO_x, which yields bad conditions and in turn keep NO destruction relatively low. Besides, the occurrence of bad high-NO conditions is reduced at high UV (bottom panels in Fig. 4), which can be explained by lowered NO due to high O₃ production and fast OH reactant loss due to high OH production. Good high-NO conditions are rare in the explored space. They are only 1.1% of total explored conditions (Fig. 3b) and present under very specific conditions, i.e., higher H₂O, lower UV, lower OHR_{ext}, and NOⁱⁿ of tens to hundreds of ppb (Figs. 4 and S5). Since a very high NO can suppress OH, to obtain both a significant NO level and a good conditions, NOⁱⁿ can only be tens to hundreds of ppb. As NOⁱⁿ is lower and OH is higher than under bad high-NO conditions, UV should be lower than bad high-NO conditions to keep a sufficiently long presence of NO. Thus, UV at 185 nm for good high-NO conditions are generally lower than 10¹² photons cm⁻² s⁻¹ (Fig. S5). In addition, a low OHR_{ext} (generally <50 s⁻¹) and a higher H₂O (the higher the better, although there is no apparent threshold) are also required for good high-NO conditions (Fig. S5), as Peng et al. (2016) pointed out. Risky high-NO conditions often occur between good and bad high-NO conditions, e.g., at lower NOⁱⁿ than bad conditions (e.g., Cases ML, MM, HL, and HM in Fig. 4, see Table 2 for the typical case label code), at higher OHR_{ext} and/or NOⁱⁿ than good conditions (e.g., Cases ML and MM), and at lower H₂O than good conditions (e.g., Case LL).

The trend of the distributions of good, risky, and bad low-NO conditions is generally in line with the analysis in Peng et al. (2016). For low-NO conditions, NO_y species can be simply regarded as external OH reactants, as in Peng et al. (2016). As H₂O decreases and/or OHR_{ext} or NOⁱⁿ increases, a low-NO condition becomes worse (good→risky→bad) (Figs. 4 and 5). In OFR185-iNO, increasing UV generally makes a low-NO condition better because of an OH production enhancement (Fig. 4); while in OFR254-iNO, increasing UV generally makes a low-NO condition worse (Fig. 5), since at a higher UV, more O₃ is destroyed and the resilience of OH to suppression is reduced.

As discussed above, the fraction of high-NO conditions also depends on OFR residence time. A shorter residence time is expected to generally lead to a larger fraction of high-NO conditions, since the time spent in the reaction for $t > \tau_{NO}$ is significantly smaller. Thus, we also investigate an OFR185-iNO case with a residence time of 30 s. In Fig. 3b, compared to the case with a residence time of 3 min, the distributions of all condition types (good/risky/bad) of the 30 s residence time case shift toward higher $r(\text{RO}_2+\text{NO})/r(\text{RO}_2+\text{HO}_2)$.

Nevertheless, shortening the residence time also removes the period when the condition is better (i.e., less non-tropospheric photolysis), when external OH reactants have been partially consumed and OH suppression due to OHR_{ext} has been reduced later in the residence time. As a result, the fractions of good and risky conditions decrease (Fig. 3b). With the two effects (higher $r(\text{RO}_2+\text{NO})/r(\text{RO}_2+\text{HO}_2)$ and more significant non-tropospheric photolysis) combined, the fraction of good high-NO conditions increases by a factor of ~3. An even shorter residence time does not result in a larger good high-NO fraction, since the effect of enhancing non-tropospheric photolysis is even more apparent.”

R1.1) The authors have to define “non-tropospheric” photolysis, which shows up as early as in the abstract, but is never properly defined. Is the connotation of stratospheric or mesospheric photolysis intended?

185 and 254 nm photons, the main driver of OH production in OFRs, do not exist in the troposphere. VOC photolysis at these wavelengths can only occur above the troposphere. We thus call it “non-tropospheric”.

We have modified the following sentence in L79 to include a clarification of non-tropospheric photolysis:

“Peng et al. (2016) systematically examined the relative importance of non-OH/non-tropospheric reactants on the fate of VOCs over a wide range of conditions, and provided guidelines for OFR operation to avoid non-tropospheric VOC photolysis, i.e., VOC photolysis at 185 and 254 nm.”

R1.2) Why have the authors chosen the term “risky” for conditions that are not unambiguously good or bad? What is the “risk” that is taken here? It would be helpful to briefly motivate the use of this word around l. 171.

We choose the word “risky” for conditions that are not unambiguously good or bad for experiments with *all* SOA precursors. Under risky conditions, some VOCs may have significant non-tropospheric photolysis while others may not. To further clarify the good/risky/bad conditions, we have modified the text in L172 to read:

“Under good conditions, photolysis of most VOCs has a relative contribution <20% to their fate; under bad conditions, non-tropospheric photolysis is likely to be significant in all OFR experiments, since it can hardly be avoided for oxidation intermediates, even if the precursor(s) does not photolyze at all. Under risky conditions, some species photolyzing slowly and/or reacting with OH rapidly (e.g., alkanes, aldehydes, and most biogenics) still have a relative contribution of photolysis <20% to their fates, while species photolyzing more rapidly and/or reacting with OH more slowly (e.g., aromatics and other highly conjugated species and some saturated carbonyls) will undergo substantial non-tropospheric photolysis. Note that these definitions are slightly different than in Peng et al. (2016).”

R1.3) Fig. 2: What is shown on the x-axis? Please label/explain these cases. This is also relevant in the later discussion, around I. 323.

We believe that the meaning of the typical case labels have been well defined in Table 2. For more clarity, we have modified the following text to better refer readers to that table.

In L150:

“We explore physical input cases evenly spaced in a logarithmic scale over very wide ranges: H₂O of 0.07%–2.3%, i.e., relative humidity (RH) of 2–71% at 295 K; 185 nm UV of 1.0x10¹¹–1.0x10¹⁴ and 254 nm UV of 4.2x10¹³–8.5x10¹⁵ photons cm⁻² s⁻¹; OHR_{ext} of 1–16000 s⁻¹; O_{3,in} of 2.2–70 ppm for OFR254; initial NO mixing ratio (NOⁱⁿ) from 10 ppt to 40 ppm. Besides, conditions with OHR_{ext}=0 are also explored. UV at 254 nm is estimated from that at 185 nm according to the relationship determined by Li et al. (2015). Several typical cases within this range as well as their corresponding 4 or 2-character labels (e.g., MM0V and HL) are defined in Table 2.”

In L319:

“In addition, a low OHR_{ext} (generally <50 s⁻¹) and a higher H₂O (the higher the better, although there is no apparent threshold) are also required for good high-NO conditions (Fig. S4), as Peng et al. (2016) pointed out. Risky high-NO conditions often occur between good and bad high-NO conditions, e.g., at lower NOⁱⁿ than bad conditions (e.g., Cases ML, MM, HL, and HM, see Table 2 for the typical case label code), at higher OHR_{ext} and/or NO_{in} than good conditions (e.g., Cases ML and MM), and at lower H₂O than good conditions (e.g., Case LL).”

In the caption of Fig. 2 (L756):

“Figure 2. Relative variances (left axes)/uncertainties (right axes) of several outputs (i.e., NO, NO₃, and OH exposures) of Monte Carlo uncertainty propagation, and relative contributions of key reactions to these relative variances in several typical cases (denoted in 4-character labels, see Table 2 for the typical case label code) in OFR185-iNO.”

R1.4) I. 295: You compare NO lifetime to reactor residence time. Should it not be better to compare to e.g. VOC lifetime in the reactor, or generally to total overturn of reactive material? I can imagine a scenario where NO is used up very quickly, but so are all other reactive gases, so that much of the reactor residence time is not used to make (or age) SOA and hence mostly irrelevant anyhow

We do not agree that a situation where “much of the reactor residence time is not used to make (or age) SOA and hence mostly irrelevant anyhow” after NO is used up quickly is likely. Even for

primary VOCs with lifetimes comparable with or shorter than that of NO, their oxidation intermediates/products actually have significant presence for a much longer period than NO lifetime (Nehr et al., 2014; Schwantes et al., 2017). Besides, heterogeneous OA oxidation can be important at high photochemical ages in OFR (Hu et al., 2016), leading to decomposition and revolatilization of particle-phase species. Whether RO₂ generated from these second and later generation species undergo high-NO or low-NO oxidation still matters in OFR chemistry, regardless of NO lifetime. Therefore, we believe that the entire residence time is the appropriate period of interest for the high/low-NO considerations.

In addition, we have investigated a case with much shorter residence time (30 s) to more focus on NO and primary VOC oxidation, as the further oxidation is limited by the short residence time. This case may be seen as closer to the Referee's scenario. However, the fraction of good high-NO conditions in this case is still comparable to that with a residence time of 180 s.

For more clarity, we have added the following sentence at the end of the first paragraph of Section S1 (L94 in SI):

“The entire residence time is taken into account since there is still significant presence of VOCs after NO and primary VOCs are destroyed. The oxidation intermediates/products of primary VOCs can exist for a much longer period than NO lifetime (Nehr et al., 2014; Schwantes et al., 2017). In addition, heterogeneous OA oxidation can be important at high photochemical ages in OFR (Hu et al., 2016), leading to decomposition and revolatilization of particle-phase species. Thus continuing oxidation processes are very likely to occur during the entire the residence time.”

R1.5) I. 299: Figure 3 is very complex, yet is doesn't find much introduction. Please expand your discussion of this figure the first time it is referenced in the text

To introduce Fig. 3, we modify the text to L298 to read:

“Figure 3 shows the fractional occurrence distribution of good/risky/bad conditions in the entire explored condition space over logarithm of $r(\text{RO}_2+\text{NO})/r(\text{RO}_2+\text{HO}_2)$, which distinguishes high- and low-NO conditions. In OFR254-iNO, t_{NO} is so short that no good high-NO condition is found in the explored range in this study (Fig. 3a).”

R1.6) I. 40: “on similar timescales”

Corrected as the Referee suggested.

R1.7) I. 41: Is there an “of” missing after “decoupling”? Alternatively: “... to decouple ...”

We have added “of” after “decoupling” and now the sentence reads:

“Chemical reactors allow for decoupling of these two types of processes.”

R1.8) l. 72: Please give a unit of exposure. Also relevant e.g. in line 197.

We have specified the units of all key quantities mentioned in this paragraph as well as in L197.

The modified text in L71 reads:

“Li et al. (2015) and Peng et al. (2015) developed a box model for OFR HO_x chemistry that predicts measurable quantities [e.g., OH exposure (OH_{exp}, in molecules cm⁻³ s) and O₃ concentration (abbr. O₃ hereinafter, in ppm)] in good agreement with experiments. This model has been used to characterize HO_x chemistry as a function of H₂O mixing ratio (abbr. H₂O hereinafter, unitless), UV light intensity (abbr. UV hereinafter, in photons cm⁻² s⁻¹), and external OH reactivity [in s⁻¹, $\text{OHR}_{\text{ext}} = \sum k_i c_i$, i.e., the sum of the products of concentrations of externally introduced OH-consuming species (c_i) and rate constants of their reactions with OH (k_i)].”

And that around L197:

“We evaluate this issue below by calculating NO effective lifetime (τ_{NO} , in s), defined as NO exposure (NO_{exp}, in molecules cm⁻³ s) divided by initial NO concentration, under various conditions.”

R1.9) l. 275: Instead of “similar with those cases” it must read “similar to those cases”.

Corrected as the Referee suggested.

R1.10) l. 394: “Despite its double bond, ethene reacts as slowly with NO₃ as alkanes, likely due to lack of alkyl groups enriching electron density on the C=C bond, which slows NO₃ addition.”
Why is this relevant here?

In that text we explained why ethene is different from other alkenes. Readers can thus get the message that NO₃ reacts rapidly with species with C=C bond, except ethene. It is not rigorous to draw the conclusion that alkenes react rapidly with NO₃ without mentioning this exception.

R1.11) l. 439-441: This sentence is confusing, the word “process” seems out of place here.

We rewrite the sentence as follows:

“As a result of $\text{NO}_{3\text{exp}}/\text{OH}_{\text{exp}} \sim 100$, only a minor portion of cresol could have undergone OH addition and then H-elimination again. This pathway leads to the formation of methyldihydroxybenzenes and other OH-oxidation products (Atkinson and Arey, 2003).”

R1.12) l. 444-447: In this sentence, please briefly state again (maybe in parenthesis) which route is which in this example (H-abstraction vs. OH addition) to avoid confusion.

We have stated the pathways in parenthesis and the text in L444 now reads:

“In summary, the model results suggest that there were two possible routes leading to nitroaromatic formation. However, one of them (recombination of OH-aromatic adducts with NO_2) is likely of little atmospheric relevance due to very high NO_x needed, and the other (H-abstraction from cresol) occurs in the atmosphere but is not a major fate of aromatics (Calvert et al., 2002).”

R1.13) l. 465: “... suppression can as high ...” should read “... suppression can be as high... ”.

Corrected as the Referee suggested.

R1.14) l. 477: “most hot stabilized period”. Is there a word missing here?

The corrected sentence reads:

“A dilution by a factor of 12, as actually used by Karjalainen et al. (2016), appears to be sufficient to bring most of the hot stabilized period under good conditions (Fig. S9).”

R1.15) Fig. S1: please use consistent colors for chemical species.

Having double-checked, we think that colors for species in Fig. S1 are consistent. In all panels of Fig. S1, all the species concentrations (or concentration ratio) have one-to-one correspondence with line styles/colors.

Anonymous Referee #2

The current paper explores a chemical space extended to consider high NO concentrations within an OFR. Such a contribution, whilst of limited interest outside the immediate field, should be of considerable worth to users of such devices, particularly those looking to explore the emissions from high temperature combustion sources. However, to some degree, the paper is missing the same point that many previous theoretical characterisations of the devices also miss. The chemical space is just one element influencing the performance and atmospheric relevance of all PAM-type reactors (and the gas phase chemical space, just a subset of this). It is for this reason that I would hope that the current study is envisaged as one of a series of papers that will be extended to the dynamical, physical and condensed-phase chemical considerations. I will return to this below.

Having said this, within the stated scope, this paper carries a large amount of good new work that will make it worthy of publication in ACP. The chemical modelling appears appropriate with most of the necessary rate constants relatively well-constrained. This allows the characterisation of "good", "risky" and "bad" conditions under both 185 and 254 nm photolysis, though with the same caveats to the earlier work relating to uncertainties in the photolysis cross-sections and product yields of all possible VOCs (particularly when considering complex mixtures as in combustion emissions). In general, I am in agreement with the other referee that the gas phase chemical modelling alone warrants publication in ACP, but would invite the authors to address two main points to establish the validity of the approach and one point relating to the contextualisation of their study.

R2.1) Validity of the plug flow assumption: in section 3.1.3 it is stated that the uncertainties relating to kinetic parameters are relatively low compared to other factors including the plug flow assumption, referring to Peng et al., 2015. It would be useful for the authors to discuss whether the relative kinetic vs dynamic uncertainties under the high NO_x conditions are of a comparable magnitude to those under low NO_x conditions. There have been plenty of studies of axial and radial gradients in flow reactors, so some justification of the highly simplified modelling approach would be appropriate, given the biggest uncertainties are explicitly stated as being related to this assumption.

We have investigated the impacts of a residence time distribution (RTD) measured by Lambe et al. (2011). Under most conditions, the difference between OH_{exp} from the plug-flow and RTD models is relatively small (within a factor of 3), while at high UV, OH_{R_{ext}}, and NOⁱⁿ, the difference can be larger. All main conclusions in this paper still hold after the discussions about the RTD impacts are included.

We have added Section 3.3 for discussion of RTD effects:

“3.3 Effect of non-plug flow

We performed model runs where the only change with respect to our box model introduced in Section 2.2 is that the plug-flow assumption is replaced by the residence time distribution (RTD) measured by Lambe et al. (2011) (also see Fig. S8 of Peng et al. (2015)). The chemistry of different air parcels with different residence times is simulated by our box model and outputs are averaged over the RTD. Lateral diffusion between different air parcels is neglected in these simulations.

OH_{exp} calculated from the model with RTD ($OH_{exp,RTD}$) is higher than that calculated from the plug-flow model ($OH_{exp,PF}$) in both OFR185-iNO and OFR254-iNO (Table 4 and Fig. S6). Under most explored conditions deviations are relatively small, which leads to an overall positive deviation of $OH_{exp,RTD}$ from $OH_{exp,PF}$ by $\sim x2$ (within the uncertainties of the model and its application to real experimental systems). For OFR185-iNO, most conditions ($\sim 90\%$) in the explored space lead to $<x3$ differences between $OH_{exp,PF}$ and $OH_{exp,RTD}$, while for a small fraction of cases the differences can be larger (Fig. S6). The larger deviations are mainly present at high UV, OHR_{ext} , and NO^{in} , where conditions are generally “bad” and in which experiments are of little atmospheric relevance. Under these specific conditions, external OH reactants and NO_y can be substantially destroyed for the air parcels with residence times longer than the average, while this is not the case for the average residence time. This feature was already described by Peng et al. (2015) (see Fig. S10 of that study). Although only non- NO_y external OH reactants were considered in that study, the results are the same. In the present study, a higher upper limit of the explored OHR_{ext} range (compared to Peng et al., 2015, due to trying to simulate extremely high OHR_{ext} used in some recent literature studies) large amounts of NO_y and cause somewhat larger deviations. In OFR254-iNO, OH is less suppressed at high OHR_{ext} and NO^{in} than in OFR185-iNO because of high O_3 (Peng et al., 2015), $OH_{exp,RTD}$ deviations from $OH_{exp,PF}$ are also smaller (Table 4).

Table 4. Statistics of the ratio between OH exposures calculated in the model with the Lambe et al. (2011) residence time distribution ($OH_{exp,RTD}$) and in the plug-flow model ($OH_{exp,PF}$). The geometric mean, uncertainty factor (geometric standard deviation), and percentage of outlier cases (>3 or $<1/3$) are shown for OFR185-iNO, OFR254-70-iNO, and OFR254-7-iNO.

	Geometric mean	Uncertainty factor	Outlier cases (%)
OFR185-iNO	1.91	1.64	11
OFR254-7-iNO	1.59	1.51	7
OFR254-70-iNO	1.48	1.29	3

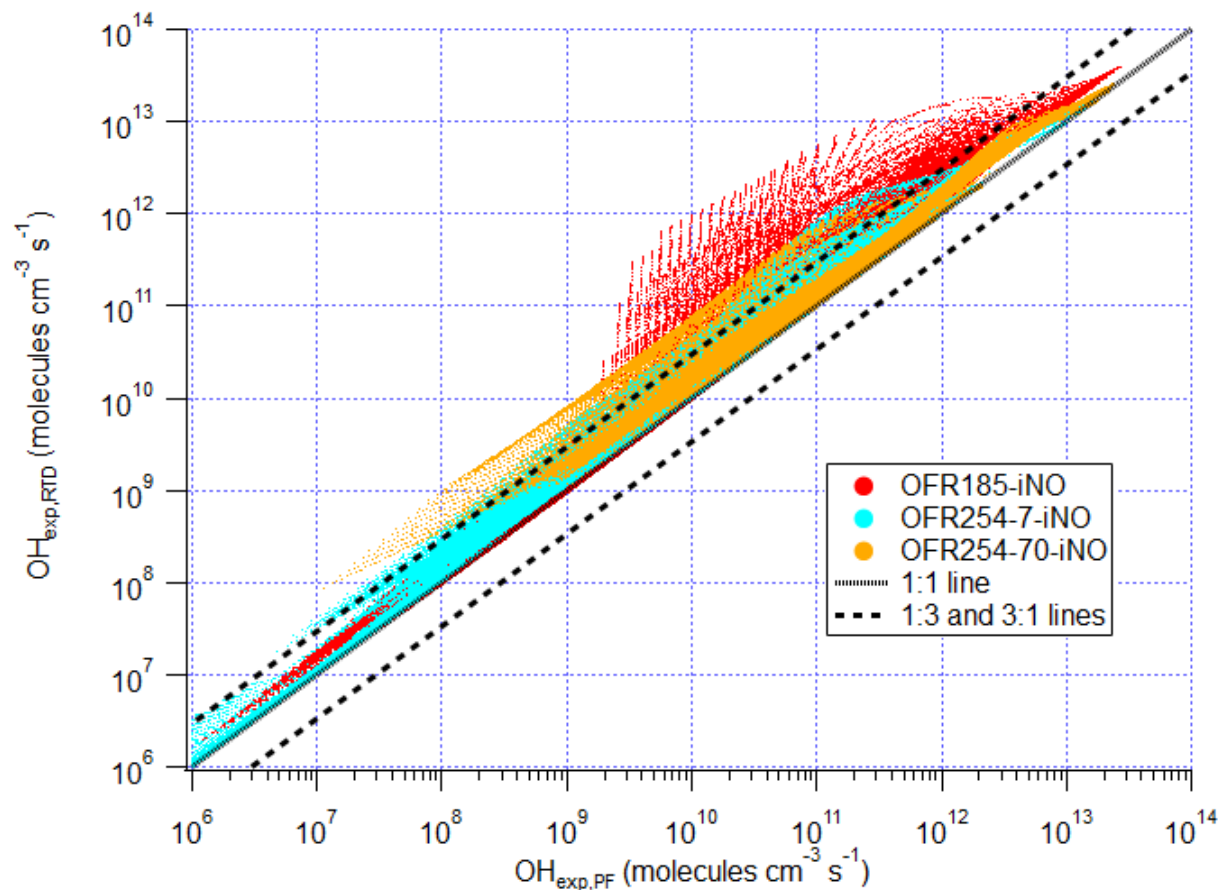


Figure S6. Scatter plot of OH exposure calculated in the model with the Lambe et al. (2011) residence time distribution ($OH_{exp,RTD}$) vs. that calculated in the plug-flow model ($OH_{exp,PF}$) for OFR185-iNO, OFR254-7-iNO, and OFR254-70-iNO. 1:1, 1:3, and 3:1 lines are also shown for comparison.

Based on the outputs of the model with RTD, similar mapping of the physical input space as Figs. 4 and 5 can be done (Figs. S7 and S8). Overall, the mapping of the RTD model results is very similar with that of the plug-flow model. The conditions appear to be only slightly better in a few places of the explored space than those from the plug-flow model, which can be easily explained by the discussions above. Besides, the mapping in Figs. S7 and S8 also appear to be slightly more low-NO, for the same reasons discussed above. After NO is destroyed at long residence times, HO_2 , suppressed by NO, also recovers as OH. $r(RO_2+NO)/r(RO_2+HO_2)$ is obviously expected to be smaller than in the plug-flow model in general.

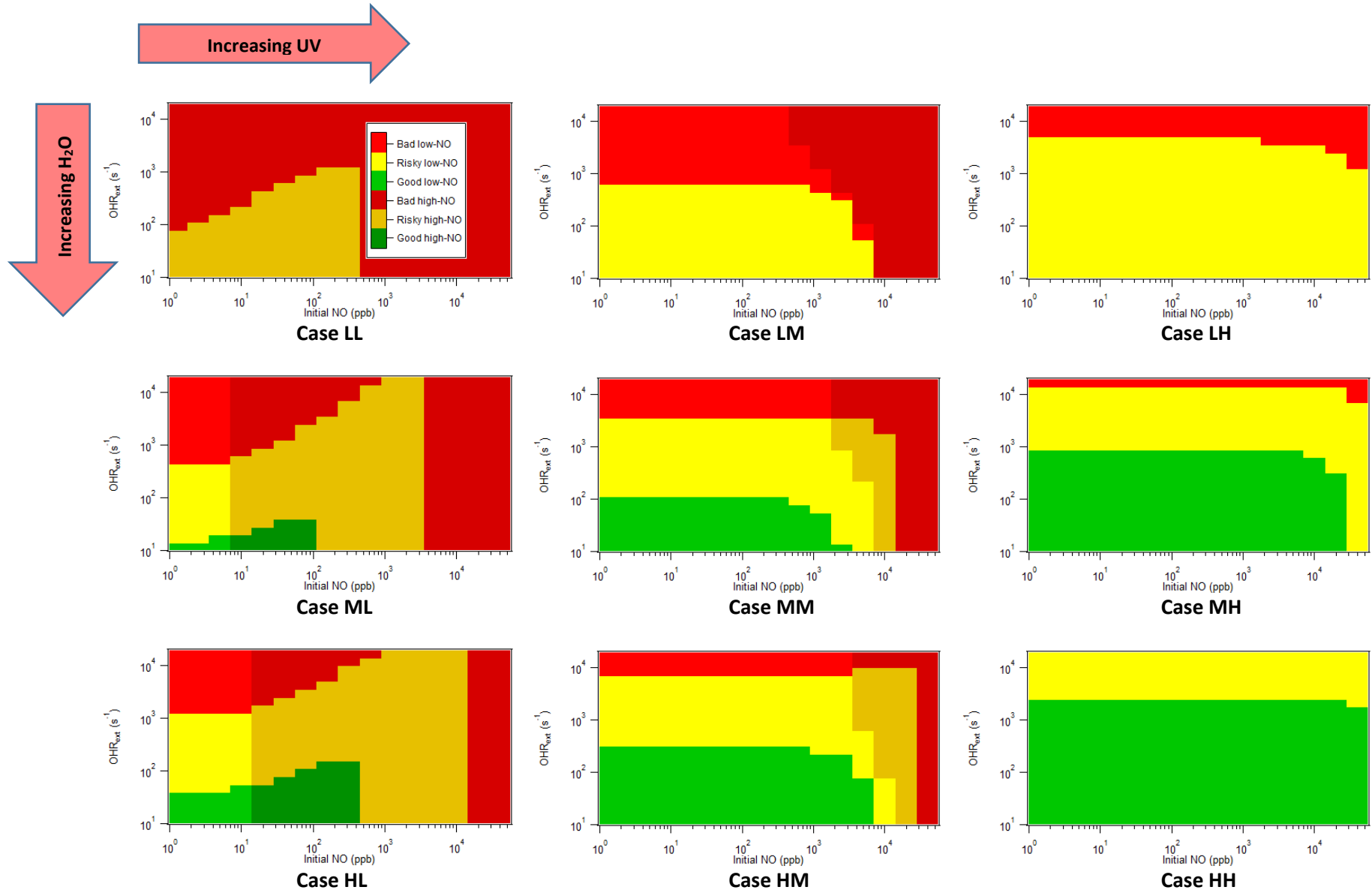


Figure S7. Same format as Fig. 4, but for the OFR185-iNO results obtained by the model with the Lambe et al. (2011) residence time distribution.

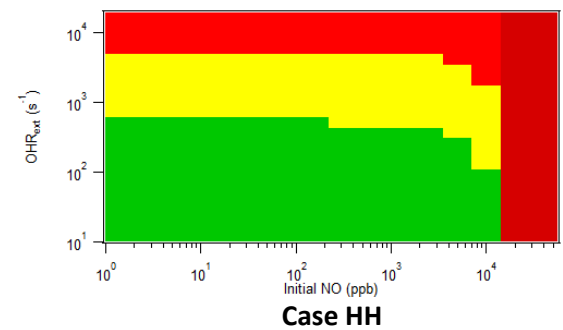
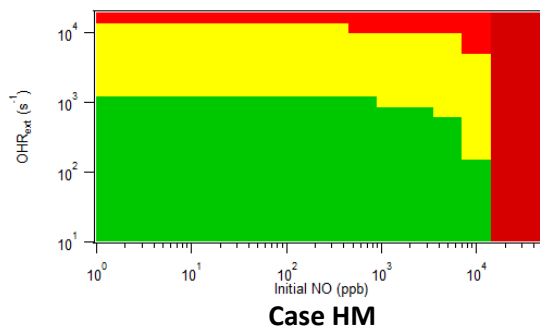
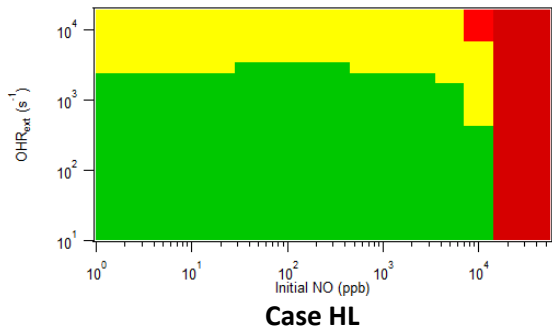
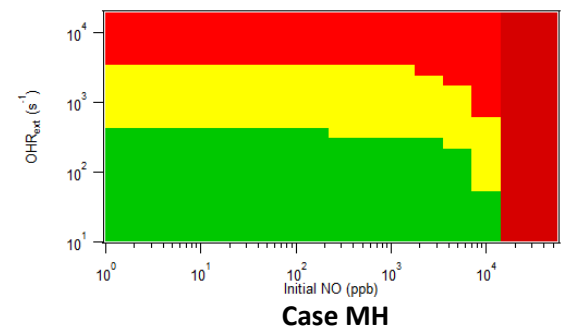
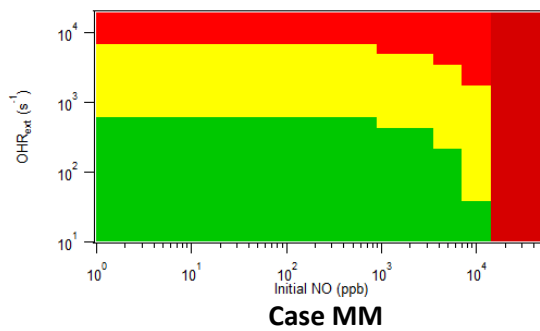
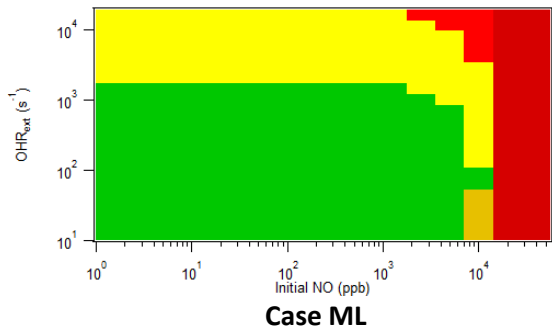
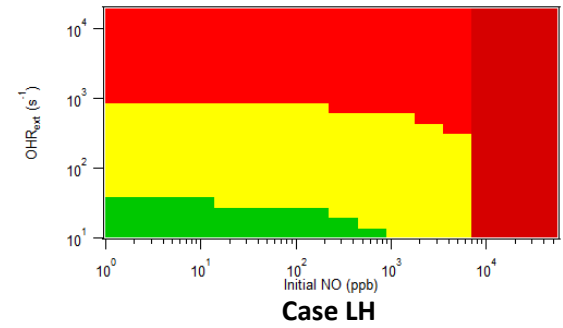
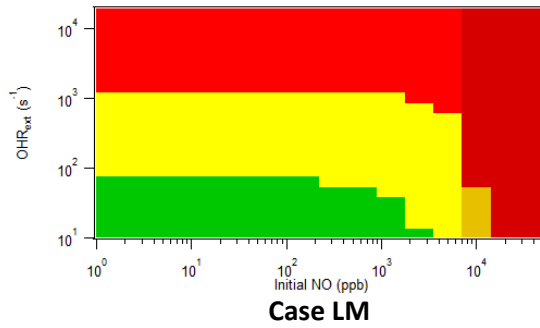
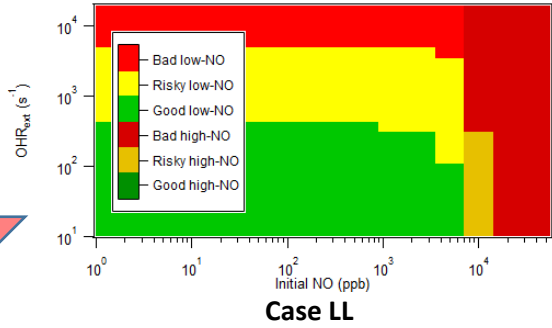
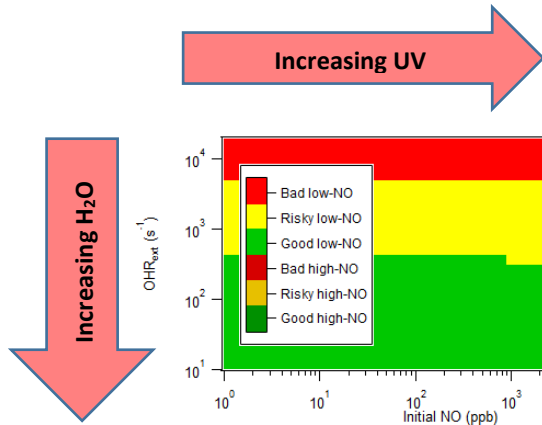


Figure S8. Same format as Fig. 5, but for the OFR254-22-iNO results obtained by the model with the Lambe et al. (2011) residence time distribution.

Note that most conditions that appear to be better in the RTD model results are already identified as bad by the plug-flow model. Those conditions look slightly better only because of their better $RTD\text{-averaged } F185_{\text{exp}}/OH_{\text{exp}}$ and $F254_{\text{exp}}/OH_{\text{exp}}$. However, each of those cases is actually composed of both a better part at longer residence times and also a worse part at shorter residence times. Under those conditions, the reactor simultaneously works in two distinct regimes, one of which is bad due to heavy OH suppression. Such conditions are obviously not desirable for OFR operation.”

R2.2) Validity of separating the numerical treatment of gas phase and particle phase processes: there is no statement of any of the uncertainty in gas phase chemistry being attributable to multiphase processes. I find this rather curious, since the primary focus of most PAM chamber studies relates to particulate mass. Both radical and closed shell species may interact substantially with the particle phase. All the particulate material in SOA particles is, by definition, formed from the vapour phase. If the flow regime is anything near plug flow, then the particle number, condensation sink, mass and composition of the particulate will evolve with the gas phase species and hence mass transfer (in both directions, where there is oxidative fragmentation and functionalisation) will be changing temporally and spatially inside the reactor. There really should be some discussion of the potential impacts of these processes in the paper.

We believe that separation of gas-phase and particle phase processes can only have minor impacts on both gas-phase and particle-phase chemistries in OFR and is thus a valid approximation.

We have modified the text to L144 to provide some discussion of this issue:

“As in Peng et al. (2015, 2016), SO_2 is used as a surrogate of external OH reactants (e.g., VOCs). NO_y species, although also external OH reactants, are explicitly treated in the model and *not* counted in OHR_{ext} in this work. Therefore, OHR_{ext} stands for *non- NO_y* OHR_{ext} only hereinafter, unless otherwise stated. Also, particle-phase processes and interactions of gas-phase species with particles are not considered in this study. We have made this assumption because:

- i) The presence of aerosols has typically negligible impacts on the gas-phase chemistry. Condensational sink (CS) of ambient aerosols can rarely exceed 1 s^{-1} even in polluted areas and is usually 1-3 orders of magnitude lower (Donahue et al., 2016; Palm et al., 2016). Thus, even under the assumption of unity uptake coefficient, CS cannot compete with OHR_{ext} (usually on the order of 10 s^{-1}) in OH loss. Uptake of NO onto aerosols only occurs through the reaction with RO_2 on particle surface (Richards-Henderson et al., 2015), which is formed very slowly (see below) compared to gas-phase HO_x and NO_x chemistry. Uptake of HO_2 , O_3 , NO_3 etc. is even more unlikely to be efficient (Moise and Rudich, 2002; Moise et al., 2002; Hearn and Smith, 2004; Lakey et al., 2015).

- ii) On the other hand, gas-phase species have only limited impacts on OA. Heterogeneous oxidation of OA by OH is generally slow. Significant OA loss due to heterogeneous oxidation can only be seen at photochemical ages as high as weeks (Hu et al., 2016). The enhancement of heterogeneous oxidation due to NO is remarkable only at OH concentration close to the ambient values but not at typical values in OFR (Richards-Henderson et al., 2015).

It is an important approximation that the *real* OHR_{ext} decay (due to not only primary VOC oxidation and subsequent oxidation, but also wall loss, partitioning to the particle phase, reactive uptake etc.) is surrogated by that of SO_2 . Gas-phase measurements in literature laboratory studies revealed that there is a large variability of total OHR_{ext} during (subsequent) oxidation of VOCs, depending on the type of precursors (Nehr et al., 2014; Schwantes et al., 2017). This variability is obviously mainly due to the evolution of different types of oxidation intermediates/products contributing to OHR_{ext} , but not due to changes in CS, wall conditions etc. Also this variability is difficult to accurately capture even if modeling with a mechanism as explicit as MCM is performed (Schwantes et al., 2017). It is thus justified to use a lumped surrogate to model the OHR_{ext} decay for simplicity and efficiency. The uncertainties introduced by this approximation include those due to both the types of oxidation intermediates/products and all interactions of VOCs with aerosols, walls etc. And the uncertainties due to the former dominate over those due to the latter.”

R2.3) My final point relates to the context of the study. If it is not envisaged that this second paper on the chemical characterisation of OFRs is to eventually be accompanied by a numerical study of the multiphase processes, then I think the paper requires quite a bit more contextualisation. The root of the missing material relates to the competition between processes (nucleation, condensation, evaporation, coagulation, condensed phase reaction) alluded to in point ii) above and relating to aerosol dynamical evolution that are highly dependent on the magnitudes of different moments of the aerosol distribution. Extrapolation to concentration regimes other than the dilutions under the operating conditions of the OFR is simply not possible without the adoption of substantial questionable assumptions or use of a highly complex model which has yet to be described. The current paper implicitly aims to limit its scope to gas phase oxidation of VOCs in the OFR, but this is seldom the purpose to which they are put. Indeed, the limited context for OFR studies explicitly points to their use for "...secondary organic aerosol (SOA) formation and aging [studies], in both the laboratory and the field", because of the perceived advantage of elevated oxidant levels. None of the disadvantages that are related directly to the inappropriate extrapolation of all the multiphase processes of relevance to SOA formation and transformation are mentioned. This requires significant rebalancing, ideally quantitatively in a further detailed publication but at least qualitatively in the introduction of the current paper.

First of all, a reactor such as an OFR is complex and can involve gas, heterogeneous, particle-phase chemistry, gas-particle partitioning thermodynamics and kinetics, size distribution dynamics, three-dimensional flow fields and UV light distributions, different wall materials, and small temperature non-uniformities in some cases. In addition, an OFR can be used in a multitude

of configurations and input conditions. It is impossible to investigate all the processes in a single paper, especially when some of the processes (e.g. the impact of high initial NO in the gas-phase chemistry in OFRs) had never been investigated before. Our approach has been to tackle important parts of the overall phase space in individual papers. In particular we are focusing on the gas-phase chemistry in several of our papers because (1) there seems to be limited understanding of it in the OFR community, (2) at least some literature studies may have been conducted under conditions far from atmospheric relevance; and (3) once this chemistry is understood, there are relatively easy and practical ways to plan experiments to avoid major problems, and to quantify the relative effects of different processes. We are working on additional manuscripts and we hope to continue to be active in this area, but overall OFR modeling is a subfield in itself, and our group cannot be expected to address every single possible topic. Even for environmental chambers, which have been around for over 6 decades, very few modeling publications consider the gas and particle chemistry and size distribution dynamics simultaneously.

Importantly, we would like to let the Referee know that we are currently collaborating with the group of Jeffrey Pierce at Colorado State University on detailed aerosol dynamics modeling in OFR, including nucleation, condensation, and coagulation, as well as heterogeneous chemistry, and our collaborators have already presented some preliminary results (Hodshire et al., 2017).

As stated in Hu et al. (2016), “the OFR does not accelerate processes such as aerosol uptake and reactions that do not scale with OH”. This feature of OFR is rather straightforward. None of aerosol dynamical processes except the uptake of species with elevated concentrations (OH, HO₂ etc.) relative to those in the atmosphere are enhanced in OFR. The short residence times and high LVOC production rates may prevent SOA growth from reaching equilibrium (Palm et al., 2016; Ahlberg et al., 2017). Also, common particle-phase chemical reactions (e.g., carbonyl-amine browning (Haan et al., 2009) and cyclic hemiacetal formation and dehydration (Strollo and Ziemann, 2013)) do not involve OH and are not accelerated in OFR. Heterogeneous OA oxidation by OH is accelerated but its main pathways are identical to those in the gas phase (Houle et al., 2015; Richards-Henderson et al., 2015) and is not as important as the gas-phase radical chemistry in terms of species production and consumption amounts (see response to R2.2). Therefore, we had not intended to limit the scope of this paper within the gas phase. As the title of this paper reads, we focus on OFR chemistry with NO, but for the reasons above, a gas-phase model is sufficient to investigate the main features of this chemistry.

Most importantly, “atmospheric relevance” in this paper does not refer to a perfect reproduction of all processes of interest in the atmosphere, as none of the reactors used for atmospheric chemistry and aerosol research can achieve this. We aim to understand the chemistry in the reactor to enable us and others to avoid the processes that do not occur in the atmosphere, and to understand the deviations in the relative importance of the processes that do occur. In OFR, aerosol dynamics may be relatively slower, compared to accelerated reactions with OH, even though both occur in both OFR and the atmosphere. Specific input conditions and/or measures of intervention may be adopted to modify and/or investigate such issues. For instance, pure sulfuric acid particles may be used to enhance the reactive uptake of IEPOX (Hu et al., 2016); or

seed particles may be injected to avoid over-oxidation of LVOCs in the gas phase before their condensation onto particles (Palm et al., 2016).

In summary, we believe that the scope of this paper and the use of a gas-phase model in this paper are appropriate, and a detailed investigation of particle-related processes, which is ongoing, will result in a future paper.

R2.4) Related to the above, the previous findings of nitrogen being incorporated into SOA are very tricky to interpret. The recommendations for operation are made from the perspective of gas phase oxidation to ensure that the gas phase product distribution is not anomalous. Incorporation of the nitrogenous species into particles will be subject to multiphase processes leading to net mass transfer between the phases. The mass transfer rate will be proportional to not only the difference between the gaseous concentration and the equilibrium concentration above the particle, but also to the condensation sink provided by the particles. Extrapolation to the amount of a component or class of components in the SOA (e.g. nitrogen-containing ones) to ambient conditions should not only consider the equivalent oxidant dose and gas phase chemical regime, but also aim to establish some equivalence in terms of the mass transfer between phases.

To our knowledge, Liu et al. (2015) is the only published OFR study reporting the incorporation of nitrogen into SOA. Their interpretation of this observation did *not* involve multiphase *chemical* processes. They interpreted their nitrogen-containing compounds observed in SOA as organic nitrates formed by $\text{RO}_2 + \text{NO}$ and nitroaromatics formed by reactions of phenoxy with NO_2 . Both pathways have been extensively discussed in our paper. In addition, we have found by modeling that under similar conditions with theirs, recombination of OH-aromatic adducts with NO_2 can be faster than that with O_2 . Since OH-aromatic adducts can be the products of the very first step of aromatic (SOA precursors in that study) oxidation, nitroaromatic formation via this pathway may be substantial (see Section 3.3.3 in the ACPD paper). All abovementioned pathways are gas-phase reactions. The products may undergo further oxidation till their volatilities are sufficiently low to condense onto aerosols.

Although it cannot be ruled out, nitrogen incorporation due to reactive uptake of NO leading to organic nitrates formation in the particle phase was found to be negligible (Richards-Henderson et al., 2015). Therefore we do not agree with the Referee that complex multiphase mass transfer considerations are necessary to interpret nitrogen incorporation into OA, at least from current experimental reports.

References (for responses to both reviewers)

- Ahlberg, E., Falk, J., Eriksson, A., Holst, T., Brune, W. H., Kristensson, A., Roldin, P. and Svenningsson, B.: Secondary organic aerosol from VOC mixtures in an oxidation flow reactor, *Atmos. Environ.*, 161, 210–220, doi:10.1016/j.atmosenv.2017.05.005, 2017.
- Atkinson, R. and Arey, J.: Atmospheric degradation of volatile organic compounds., *Chem. Rev.*, 103(12), 4605–38, doi:10.1021/cr0206420, 2003.
- Calvert, J. G., Atkinson, R., Becker, K. H., Kamens, R. M., Seinfeld, J. H., Wallington, T. H. and Yarwood, G.: *The Mechanisms of Atmospheric Oxidation of the Aromatic Hydrocarbons*, Oxford University Press, USA. [online] Available from: <https://books.google.com/books?id=P0basaLrxDMC>, 2002.
- Donahue, N. M., Posner, L. N., Westervelt, D. M., Li, Z., Shrivastava, M., Presto, A. A., Sullivan, R. C., Adams, P. J., Pandis, S. N. and Robinson, A. L.: Where Did This Particle Come From? Sources of Particle Number and Mass for Human Exposure Estimates, in *Airborne Particulate Matter: Sources, Atmospheric Processes and Health*, edited by R. M. Harrison, R. E. Hester, and X. Querol, pp. 35–71, Royal Society of Chemistry., 2016.
- Haan, D. O. De, Corrigan, A. L., Smith, K. W., Stroik, D. R., Turley, J. J., Lee, F. E., Tolbert, M. A., Jimenez, J. L., Cordova, K. E. and Ferrell, G. R.: Secondary Organic Aerosol-Forming Reactions of Glyoxal with Amino Acids, *Environ. Sci. Technol.*, 43(8), 2818–2824, doi:10.1021/es803534f, 2009.
- Hearn, J. D. and Smith, G. D.: Kinetics and Product Studies for Ozonolysis Reactions of Organic Particles Using Aerosol CIMS †, *J. Phys. Chem. A*, 108(45), 10019–10029, doi:10.1021/jp0404145, 2004.
- Hodshire, A., Palm, B., Jimenez, J.-L., Bian, Q., Pierce, J. R., Campuzano-Jost, P., Day, D., Peng, Z., Ortega, A., Hunter, J., Cross, E., Kroll, J., Kaser, L., Jud, W., Karl, T. and Hansel, A.: Nucleation and Growth Under High Oh Conditions: Using an Oxidation Flow Reactor and the Tomas Box Model to Learn About Chemistry, Nucleation, and Growth Potential of Ambient Pine-Forest Air, in *American Association for Aerosol Research 36th Annual Conference*, p. Abstract Number: 59. [online] Available from: <http://aaarabstracts.com/2017/viewabstract.php?pid=59>, 2017.
- Houle, F. A., Hinsberg, W. D. and Wilson, K. R.: Oxidation of a model alkane aerosol by OH radical: the emergent nature of reactive uptake, *Phys. Chem. Chem. Phys.*, 17(6), 4412–4423, doi:10.1039/C4CP05093B, 2015.
- Hu, W., Palm, B. B., Day, D. A., Campuzano-Jost, P., Krechmer, J. E., Peng, Z., de Sá, S. S., Martin, S. T., Alexander, M. L., Baumann, K., Hacker, L., Kiendler-Scharr, A., Koss, A. R., de Gouw, J. A., Goldstein, A. H., Seco, R., Sjostedt, S. J., Park, J.-H., Guenther, A. B., Kim, S., Canonaco, F., Prévôt, A. S. H., Brune, W. H. and Jimenez, J. L.: Volatility and lifetime against OH heterogeneous reaction of ambient isoprene-epoxydiols-derived secondary organic aerosol (IEPOX-SOA), *Atmos. Chem. Phys.*, 16(18), 11563–11580, doi:10.5194/acp-16-11563-2016, 2016.
- Karjalainen, P., Timonen, H., Saukko, E., Kuuluvainen, H., Saarikoski, S., Aakko-Saksa, P., Murtonen, T., Bloss, M., Dal Maso, M., Simonen, P., Ahlberg, E., Svenningsson, B., Brune, W.

H., Hillamo, R., Keskinen, J. and Rönkkö, T.: Time-resolved characterization of primary particle emissions and secondary particle formation from a modern gasoline passenger car, *Atmos. Chem. Phys.*, 16(13), 8559–8570, doi:10.5194/acp-16-8559-2016, 2016.

Lakey, P. S. J., George, I. J., Whalley, L. K., Baeza-Romero, M. T. and Heard, D. E.: Measurements of the HO₂ Uptake Coefficients onto Single Component Organic Aerosols, *Environ. Sci. Technol.*, 49(8), 4878–4885, doi:10.1021/acs.est.5b00948, 2015.

Lambe, A. T., Ahern, A. T., Williams, L. R., Slowik, J. G., Wong, J. P. S., Abbatt, J. P. D., Brune, W. H., Ng, N. L., Wright, J. P., Croasdale, D. R., Worsnop, D. R., Davidovits, P. and Onasch, T. B.: Characterization of aerosol photooxidation flow reactors: heterogeneous oxidation, secondary organic aerosol formation and cloud condensation nuclei activity measurements, *Atmos. Meas. Tech.*, 4(3), 445–461, doi:10.5194/amt-4-445-2011, 2011.

Li, R., Palm, B. B., Ortega, A. M., Hu, W., Peng, Z., Day, D. A., Knote, C., Brune, W. H., de Gouw, J. and Jimenez, J. L.: Modeling the radical chemistry in an Oxidation Flow Reactor (OFR): radical formation and recycling, sensitivities, and OH exposure estimation equation, *J. Phys. Chem. A*, 119(19), 4418–4432, doi:10.1021/jp509534k, 2015.

Liu, P. F., Abdelmalki, N., Hung, H.-M., Wang, Y., Brune, W. H. and Martin, S. T.: Ultraviolet and visible complex refractive indices of secondary organic material produced by photooxidation of the aromatic compounds toluene and m-Xylene, *Atmos. Chem. Phys.*, 15(3), 1435–1446, doi:10.5194/acp-15-1435-2015, 2015.

Moise, T. and Rudich, Y.: Reactive Uptake of Ozone by Aerosol-Associated Unsaturated Fatty Acids: Kinetics, Mechanism, and Products, *J. Phys. Chem. A*, 106(27), 6469–6476, doi:10.1021/jp025597e, 2002.

Moise, T., Talukdar, R. K., Frost, G. J., Fox, R. W. and Rudich, Y.: Reactive uptake of NO₃ by liquid and frozen organics, *J. Geophys. Res.*, 107(D2), 4014, doi:10.1029/2001JD000334, 2002.

Nehr, S., Bohn, B., Fuchs, H., Häseler, R., Hofzumahaus, A., Li, X., Rohrer, F., Tillmann, R. and Wahner, A.: Atmospheric photochemistry of aromatic hydrocarbons: OH budgets during SAPHIR chamber experiments, *Atmos. Chem. Phys.*, 14(13), 6941–6952, doi:10.5194/acp-14-6941-2014, 2014.

Orlando, J. J. and Tyndall, G. S.: Laboratory studies of organic peroxy radical chemistry: an overview with emphasis on recent issues of atmospheric significance, *Chem. Soc. Rev.*, 41(19), 6294, doi:10.1039/c2cs35166h, 2012.

Ortega, A. M., Hayes, P. L., Peng, Z., Palm, B. B., Hu, W., Day, D. A., Li, R., Cubison, M. J., Brune, W. H., Graus, M., Warneke, C., Gilman, J. B., Kuster, W. C., de Gouw, J., Gutiérrez-Montes, C. and Jimenez, J. L.: Real-time measurements of secondary organic aerosol formation and aging from ambient air in an oxidation flow reactor in the Los Angeles area, *Atmos. Chem. Phys.*, 16(11), 7411–7433, doi:10.5194/acp-16-7411-2016, 2016.

Palm, B. B., Campuzano-Jost, P., Ortega, A. M., Day, D. A., Kaser, L., Jud, W., Karl, T., Hansel, A., Hunter, J. F., Cross, E. S., Kroll, J. H., Peng, Z., Brune, W. H. and Jimenez, J. L.: In situ secondary organic aerosol formation from ambient pine forest air using an oxidation flow reactor, *Atmos. Chem. Phys.*, 16(5), 2943–2970, doi:10.5194/acp-16-2943-2016, 2016.

Peng, Z., Day, D. A., Ortega, A. M., Palm, B. B., Hu, W., Stark, H., Li, R., Tsigaridis, K., Brune, W. H. and Jimenez, J. L.: Non-OH chemistry in oxidation flow reactors for the study of atmospheric chemistry systematically examined by modeling, *Atmos. Chem. Phys.*, 16(7), 4283–4305, doi:10.5194/acp-16-4283-2016, 2016.

Peng, Z., Day, D. A., Stark, H., Li, R., Lee-Taylor, J., Palm, B. B., Brune, W. H. and Jimenez, J. L.: HOx radical chemistry in oxidation flow reactors with low-pressure mercury lamps systematically examined by modeling, *Atmos. Meas. Tech.*, 8(11), 4863–4890, doi:10.5194/amt-8-4863-2015, 2015.

Richards-Henderson, N. K., Goldstein, A. H. and Wilson, K. R.: Large Enhancement in the Heterogeneous Oxidation Rate of Organic Aerosols by Hydroxyl Radicals in the Presence of Nitric Oxide, *J. Phys. Chem. Lett.*, 6, 4451–4455, doi:10.1021/acs.jpcclett.5b02121, 2015.

Schwantes, R. H., Schilling, K. A., McVay, R. C., Lignell, H., Coggon, M. M., Zhang, X., Wennberg, P. O. and Seinfeld, J. H.: Formation of highly oxygenated low-volatility products from cresol oxidation, *Atmos. Chem. Phys.*, 17(5), 3453–3474, doi:10.5194/acp-17-3453-2017, 2017.

Strollo, C. M. and Ziemann, P. J.: Products and mechanism of secondary organic aerosol formation from the reaction of 3-methylfuran with OH radicals in the presence of NOx, *Atmos. Environ.*, 77, 534–543, doi:10.1016/j.atmosenv.2013.05.033, 2013.

1 **Modeling of the chemistry in oxidation flow reactors with high initial NO**

2 Zhe Peng and Jose L. Jimenez

3 Cooperative Institute for Research in Environmental Sciences and Department of Chemistry, University of
4 Colorado, Boulder, CO 80309, USA

5 Correspondence to: J.L. Jimenez (jose.jimenez@colorado.edu)

6

7 **Abstract.** Oxidation flow reactors (OFRs) are increasingly employed in atmospheric chemistry research
8 because of their high efficiency of OH radical production from low-pressure Hg lamp emissions at both
9 185 and 254 nm (OFR185) or 254 nm only (OFR254). OFRs have been thought to be limited to studying
10 low-NO chemistry (where peroxy radicals (RO₂) react preferentially with HO₂) because NO is very rapidly
11 oxidized by the high concentrations of O₃, HO₂, and OH in OFRs. However, many groups are performing
12 experiments aging combustion exhaust with high NO levels, or adding NO in the hopes of simulating
13 high-NO chemistry (where RO₂ + NO dominates). This work systematically explores the chemistry in
14 OFRs with high initial NO. Using box modeling, we investigate the interconversion of N-containing
15 species and the uncertainties due to kinetic parameters. Simple initial injection of NO in OFR185
16 can result in more RO₂ reacted with NO than with HO₂ and minor non-tropospheric photolysis, but only
17 under a very narrow set of conditions (high water mixing ratio, low UV intensity, low external OH
18 reactivity (OHR_{ext}), and initial NO concentration (NOⁱⁿ) of tens to hundreds of ppb) that account for a
19 very small fraction of the input parameter space. These conditions are generally far away from
20 experimental conditions of published OFR studies with high initial NO. In particular, studies of aerosol
21 formation from vehicle emissions in OFR often used OHR_{ext} and NOⁱⁿ several orders of magnitude higher.
22 Due to extremely high OHR_{ext} and NOⁱⁿ, some studies may have resulted in substantial non-tropospheric
23 photolysis, strong delay to RO₂ chemistry due to peroxyxynitrate formation, VOC reactions with NO₃
24 dominating over those with OH, and faster reactions of OH-aromatic adducts with NO₂ than those with
25 O₂, all of which are irrelevant to ambient VOC photooxidation chemistry. Some of the negative effects
26 are worst for alkene and aromatic precursors. To avoid undesired chemistry, vehicle emissions generally
27 need to be diluted by a factor of >100 before being injected into OFR. However, sufficiently diluted
28 vehicle emissions generally do not lead to high-NO chemistry in OFR, but are rather dominated by the
29 low-NO RO₂+HO₂ pathway. To ensure high-NO conditions without substantially atmospherically irrelevant
30 chemistry in a more controlled fashion, new techniques are needed.

Deleted: Peng^{1,2}

Deleted: Jimenez^{1,2}

Deleted: ¹

Deleted: ² Department of Chemistry and Biochemistry, University of Colorado, Boulder, CO 80309, USA

36 1 Introduction

37 The oxidation of gases that are emitted into the atmosphere, in particular volatile organic
38 compounds (VOCs), is one of the most important atmospheric chemistry processes (Haagen-Smit, 1952;
39 Chameides et al., 1988). VOC oxidation is closely related to radical production and consumption (Levy
40 II, 1971), O₃ production, and formation of secondary aerosols (Odum et al., 1996; Hoffmann et al., 1997;
41 Volkamer et al., 2006; Hallquist et al., 2009), which have impacts on air quality and climate (Lippmann,
42 1991; Nel, 2005; Stocker et al., 2014).

43 Chemical reactors are critical tools for research of VOC oxidation. Oxidation reactions of interest
44 often have typical timescales of hours to weeks. Studying these processes in ambient air can be
45 confounded by dispersion and changes in ambient conditions, which often occur on similar timescales.

46 Chemical reactors allow for decoupling of these two types of processes. Also, they should be able to
47 simulate the different regimes of reactions occurring in the atmosphere, e.g., VOC oxidation under low
48 and high-NO conditions (peroxy radical fate dominated by reaction with HO₂ or with NO) representing
49 remote and urban areas, respectively (Orlando and Tyndall, 2012).

50 Large environmental chambers are a commonly used reactor type (Carter et al., 2005; Wang et al.,
51 2011). They typically employ actinic wavelength (>300 nm) light sources (e.g., outdoor solar radiation
52 and UV blacklights) to produce oxidants and radicals and have large volumes (on the order of several
53 cubic meters or larger). However, the capability of generating sustained elevated levels of OH, the most
54 important tropospheric oxidant, is usually limited in chambers, resulting in OH concentrations similar
55 to those in the atmosphere (10⁶–10⁷ molecules cm⁻³; Mao et al., 2009; Ng et al., 2010), and consequently,
56 long simulation times (typically hours) to reach OH equivalent ages of atmospheric relevance (George
57 et al., 2007; Kang et al., 2007; Carlton et al., 2009; Seakins, 2010; Wang et al., 2011). The partitioning of
58 gases and aerosols to chamber walls (usually made of Teflon) in timescales of tens of minutes to hours
59 makes it difficult to conduct very long experiments that simulate high atmospherically-relevant
60 photochemical ages (Cocker et al., 2001; Matsunaga and Ziemann, 2010; Zhang et al., 2014; Krechmer
61 et al., 2016). In addition, the long simulation times and large size of chambers and auxiliary equipment
62 are logistically difficult for field deployment, and their cost limits the number of laboratories equipped
63 with them.

64 Given the limitations of environmental chambers, a growing number of experimenters have
65 instead employed oxidation flow reactors (OFRs). OFRs have a much smaller size (of the order of 10 L),
66 efficiently generate OH via photolysis of H₂O and/or O₃ by more energetic 185 and 254 nm photons
67 from low-pressure Hg lamps, and overcome the abovementioned shortcomings of chambers due to a
68 much shorter residence time (George et al., 2007; Kang et al., 2007, 2011; Lambe et al., 2011). Moreover,
69 OFRs are able to rapidly explore a wide range of OH equivalent ages within a short period (~2 hr), during
70 which significant changes of ambient conditions can usually be avoided in the case of field deployment
71 (Ortega et al., 2016; Palm et al., 2016, 2017). Because of these advantages, OFRs have recently been
72 widely used to study atmospheric chemistry, in particular secondary organic aerosol (SOA) formation
73 and aging, in both the laboratory and the field (Kang et al., 2011; Li et al., 2013; Ortega et al., 2013,

Deleted: in

75 2016; Tkacik et al., 2014; Palm et al., 2016).

76 In addition to experimental studies using OFRs, there has also been some progress in the
77 characterization of OFR chemistry by modeling. Li et al. (2015) and Peng et al. (2015) developed a box
78 model for OFR HO_x chemistry that predicts measurable quantities [e.g., OH exposure (OH_{exp}, in
79 molecules cm⁻³ s) and O₃ concentration (abbr. O₃ hereinafter, in ppm)] in good agreement with
80 experiments. This model has been used to characterize HO_x chemistry as a function of H₂O mixing ratio
81 (abbr. H₂O hereinafter, unitless), UV light intensity (abbr. UV hereinafter, in photons cm⁻² s⁻¹), and
82 external OH reactivity [in s⁻¹, OHR_{ext} = ∑ k_iC_i, i.e., the sum of the products of concentrations of externally
83 introduced OH-consuming species (C_i) and rate constants of their reactions with OH (k_i)]. Based on this
84 characterization, Peng et al. (2015) found that OH suppression, i.e., reduction of OH concentration
85 caused by OHR_{ext}, is a common feature under many typical OFR operation conditions. Peng et al. (2016)
86 systematically examined the relative importance of non-OH/non-tropospheric reactants on the fate of
87 VOCs over a wide range of conditions, and provided guidelines for OFR operation to avoid non-
88 tropospheric VOC photolysis, i.e., VOC photolysis at 185 and 254 nm.

89 In previous OFR modeling studies, NO_x chemistry was not investigated in detail, since in such in
90 typical OFR experiments with large amounts of oxidants (e.g., OH, HO₂, and O₃), NO would be very
91 rapidly oxidized and thus unable to compete with HO₂ for reaction with peroxy radicals (RO₂). Li et al.
92 (2015) estimated an NO (NO₂) lifetime of ~0.5 (~1.5) s under a typical OFR condition. From these
93 estimates, OFRs processing ambient air or laboratory air without large addition of NO_x were assumed
94 to be not suitable for studying oxidation mechanisms relevant to polluted conditions under higher NO
95 concentrations. OFRs have recently been used to conduct laboratory experiments with very high initial
96 NO_x levels (Liu et al., 2015) and deployed to an urban tunnel, where NO_x was high enough to be a major
97 OH reactant (Tkacik et al., 2014). The former study reported evidence for the incorporation of nitrogen
98 into SOA. Besides, OFRs have been increasingly employed to process emissions of vehicles, biomass
99 burning, and other combustion sources (Table 1), where NO can often be hundreds of ppm (Ortega et
100 al., 2013; Martinsson et al., 2015; Karjalainen et al., 2016; Link et al., 2016; Schill et al., 2016; Alanen et
101 al., 2017; Simonen et al., 2017). It can be expected that such a high NO input together with very high
102 VOC concentrations would cause a substantial deviation from good OFR operation conditions identified
103 in Peng et al. (2016). Very recently, N₂O injection has been proposed by Lambe et al. (2017) as a way to
104 study oxidation of VOCs under high NO conditions in OFR. As more OFR studies at high NO_x level are
105 conducted, there is growing need to understand the chemistry of N-containing species in OFRs and
106 whether it proceeds along atmospherically-relevant channels.

107 In this study, we present the first comprehensive model of OFR NO_y chemistry. We extend the
108 model of Li et al. (2015) and Peng et al. (2015) by including a scheme for NO_y species. Then this model
109 is used to investigate i) if an OFR with initial NO injection results in NO significantly reacting with RO₂
110 under any conditions, ii) if previously published OFR experiments with high initial NO concentrations
111 led to RO₂+NO being dominant in VOC oxidation without negative side effects (e.g., non-tropospheric
112 reactions), iii) how to avoid undesired chemistry in future studies. The results can provide insights into

Formatted: Font color: Text 1

Formatted: Font color: Text 1

Deleted:)

Formatted: Font color: Text 1

Formatted: Font color: Text 1

Formatted: Font color: Text 1

Formatted: Font color: Text 1

Formatted: Font color: Text 1

Formatted: Font color: Text 1

Formatted: Font: 9 pt, Font color: Text 1

Formatted: Font color: Text 1

Formatted: Font color: Text 1

Formatted: Font color: Text 1

Deleted: reactions

Formatted: Font color: Text 1

115 the design and interpretation of future OH-oxidation OFR experiments with large amounts of NO_x
116 injection.

117 **2 Methods**

118 The physical design of the OFR modeled in the present work, the chemical kinetics box model, and
119 the method of propagating and analyzing the parametric uncertainties on the model have already been
120 introduced previously (Kang et al., 2007; Li et al., 2015; Peng et al., 2015). We only provide brief
121 descriptions for them below.

122 **2.1 Potential Aerosol Mass flow reactor**

123 The OFR modeled in this study is the “Potential Aerosol Mass” (PAM) flow reactor, firstly
124 introduced by Kang et al. (2007). The PAM OFR is a cylindrical vessel with a volume of ~13 L, equipped
125 with low-pressure Hg lamps (model no. 82-9304-03, BHK Inc.) to generate 185 and 254 nm UV light.
126 This popular design is being used by many atmospheric chemistry research groups, particularly those
127 studying SOA (Lambe and Jimenez, 2017 and references therein). When the lamps are mounted inside
128 Teflon sleeves, photons at both wavelengths are transmitted and contribute to OH production (“OFR185
129 mode”). In OFR185, H₂O photolyzed at 185 nm produces OH and HO₂, while O₂ photolyzed at the same
130 wavelengths results in O₃ formation. O(¹D) is produced via O₃ photolysis at 254 nm and generates
131 additional OH through its reaction with H₂O. 185 nm lamp emissions can be filtered by mounting the
132 lamps inside quartz sleeves, leaving only 254 nm photons to produce OH (“OFR254 mode”). In this mode,
133 injection of externally formed O₃ is necessary to ensure OH production. As the amount of O₃ injected is
134 a key parameter under some conditions (Peng et al., 2015), we adopt the notation OFR254-X to denote
135 OFR254 experiments with X ppm initial O₃ (O_{3,in}). In this study, we investigate OFR experiments with NO
136 injected and thus utilize “OFR185-iNO” to describe the OFR185 mode of operation with initially (at the
137 reactor entrance) injected NO. The same terminology is used for the OFR254 mode. For instance, the
138 initial NO injection into OFR254-7 is denoted as OFR254-7-iNO.

139 **2.2 Model description**

140 The basic framework of the box model used in this study, a standard chemical kinetics model, is
141 the same as in Peng et al. (2015). Plug flow is assumed in the model, since approximately taking
142 residence time distribution into account leads to similar results under most conditions but at much
143 higher computational expense (Peng et al., 2015). In addition to the reactions in the model of Peng et
144 al. (2015), including all HO_x reactions available in the JPL Chemical Kinetic Data Evaluation (Sander et al.,
145 2011), all gas-phase NO_y reactions available in the JPL database except those of organic nitrates and
146 peroxy nitrates are also considered in the current reaction scheme. An updated JPL evaluation was
147 published recently (Burkholder et al., 2015), with slightly different (~20%) rate constants for
148 NO₂+HO₂+M→HO₂NO₂+M and NO₂+NO₃→N₂O₅. The updated rate constants only result in changes of
149 ~10–20% of the concentrations of the species directly consumed/produced by these reactions. These
150 changes are smaller than the parametric uncertainties of the model (see Section 3.1.3). For other
151 species, concentration changes are negligible. HO₂NO₂+M→HO₂+NO₂+M and N₂O₅+M→NO₂+NO₃+M,
152 are also included in the scheme, with kinetic parameters from the IUPAC Task Group on Atmospheric

153 Chemical Kinetic Data Evaluation (Ammann et al., 2016). As in Peng et al. (2015, 2016), SO₂ is used as a
154 surrogate of external OH reactants (e.g., VOCs). NO_y species, although also external OH reactants, are
155 explicitly treated in the model and *not* counted in OHR_{ext} in this work. Therefore, OHR_{ext} stands for *non*-
156 NO_y OHR_{ext} only hereinafter, unless otherwise stated. Also, particle-phase processes and interactions of
157 gas-phase species with particles are not considered in this study. We have made this assumption
158 because:

159 i) The presence of aerosols has typically negligible impacts on the gas-phase chemistry.
160 Condensational sink (CS) of ambient aerosols can rarely exceed 1 s⁻¹ even in polluted
161 areas and is usually 1-3 orders of magnitude lower (Donahue et al., 2016; Palm et al.,
162 2016). Thus, even under the assumption of unity uptake coefficient, CS cannot compete
163 with OHR_{ext} (usually on the order of 10 s⁻¹) in OH loss. Uptake of NO onto aerosols only
164 occurs through the reaction with RO₂ on particle surface (Richards-Henderson et al.,
165 2015), which is formed very slowly (see below) compared to gas-phase HO₂ and NO_x
166 chemistry. Uptake of HO₂, O₃, NO₃ etc. is even more unlikely to be efficient (Moise and
167 Rudich, 2002; Moise et al., 2002; Hearn and Smith, 2004; Lakey et al., 2015).

168 ii) On the other hand, gas-phase species have only limited impacts on OA. Heterogeneous
169 oxidation of OA by OH is generally slow. Significant OA loss due to heterogeneous
170 oxidation can only be seen at photochemical ages as high as weeks (Hu et al., 2016).
171 The enhancement of heterogeneous oxidation due to NO is remarkable only at OH
172 concentration close to the ambient values but not at typical values in OFR (Richards-
173 Henderson et al., 2015).

174 It is an important approximation that the *real* OHR_{ext} decay (due to not only primary VOC
175 oxidation and subsequent oxidation, but also wall loss, partitioning to the particle phase, reactive
176 uptake etc.) is surrogated by that of SO₂. Gas-phase measurements in literature laboratory studies
177 revealed that there is a large variability of total OHR_{ext} during (subsequent) oxidation of VOCs,
178 depending on the type of precursors (Nehr et al., 2014; Schwantes et al., 2017). This variability is
179 obviously mainly due to the evolution of different types of oxidation intermediates/products
180 contributing to OHR_{ext}, but not due to changes in CS, wall conditions etc. Also this variability is difficult
181 to accurately capture even if modeling with a mechanism as explicit as MCM is performed (Schwantes
182 et al., 2017). It is thus justified to use a lumped surrogate to model the OHR_{ext} decay for simplicity and
183 efficiency. The uncertainties introduced by this approximation include those due to both the types of
184 oxidation intermediates/products and all interactions of VOCs with aerosols, walls etc. And the
185 uncertainties due to the former dominate over those due to the latter.

186 A residence time of 180 s and typical temperature (295 K) and atmospheric pressure (835 mbar)
187 in Boulder, CO, USA are assumed for all model cases. The lower-than-sea level pressure only leads to
188 minor differences in the outputs (Li et al., 2015). We explore physical input cases evenly spaced in a
189 logarithmic scale over very wide ranges: H₂O of 0.07%–2.3%, i.e., relative humidity (RH) of 2–71% at
190 295 K; 185 nm UV of 1.0x10¹¹–1.0x10¹⁴ and 254 nm UV of 4.2x10¹³–8.5x10¹⁵ photons cm⁻² s⁻¹; OHR_{ext} of

191 1–16000 s⁻¹; O_{3,in} of 2.2–70 ppm for OFR254; initial NO mixing ratio (NOⁱⁿ) from 10 ppt to 40 ppm.
192 Besides, conditions with OHR_{ext}=0 are also explored. UV at 254 nm is estimated from that at 185 nm
193 according to the relationship determined by Li et al. (2015). Several typical cases within this range as
194 well as their corresponding 4 or 2-character labels (e.g., MMOV and HL) are defined in Table 2. Literature
195 studies are modeled by adopting all reported parameters (e.g., residence time, H₂O, and O_{3,in}) and
196 estimating any others that may be needed (e.g., UV) from the information provided in the papers.

197 In this study, OH equivalent ages are calculated under the assumption of an ambient OH
198 concentration of 1.5x10⁶ molecules cm⁻³ (Mao et al., 2009). Conditions leading to a ratio of RO₂ reacted
199 with NO over the entire residence time [r(RO₂+NO)] to that with HO₂ [r(RO₂+HO₂)] larger than 1 are
200 regarded as “high NO” (under the assumption of constant OHR_{ext} from VOCs, see Section S1 for more
201 details), where [r(X)] is the total reactive flux for reaction X over the entire residence time. F_{185_{exp}}/OH_{exp}
202 and F_{254_{exp}}/OH_{exp} are used as measures of the relative importance of VOC photolysis at 185 and 254
203 nm to their reactions with OH, respectively [F_{185_{exp}} (F_{254_{exp}}) are 185 (254) nm photon flux exposure,
204 i.e., product of 185 (254) nm photon flux and time]. Readers may refer to Figs. 1 and 2 of Peng et al.
205 (2016) for the determination of the relative importance of non-tropospheric (185 and 254 nm)
206 photolysis of individual VOCs. Although the relative importance of non-tropospheric photolysis depends
207 on individual VOCs, in the present work, we set criteria on F_{185_{exp}}/OH_{exp}<3x10³ cm/s and
208 F_{254_{exp}}/OH_{exp}<4x10⁵ cm/s to define “good” conditions and F_{185_{exp}}/OH_{exp}<1x10⁵ cm/s and
209 F_{254_{exp}}/OH_{exp}<1x10⁷ cm/s (excluding good conditions) to define “risky” conditions. Conditions with
210 higher F_{185_{exp}}/OH_{exp} or F_{254_{exp}}/OH_{exp} are defined as “bad”. Under good conditions, photolysis of most
211 VOCs has a relative contribution <20% to their fate; under bad conditions, non-tropospheric photolysis
212 is likely to be significant in all OFR experiments, since it can hardly be avoided for oxidation
213 intermediates, even if the precursor(s) does not photolyze at all. Under risky conditions, some species
214 photolyzing slowly and/or reacting with OH rapidly (e.g., alkanes, aldehydes, and most biogenics) still
215 have a relative contribution of photolysis <20% to their fates, while species photolyzing more rapidly
216 and/or reacting with OH more slowly (e.g., aromatics and other highly conjugated species and some
217 saturated carbonyls) will undergo substantial non-tropospheric photolysis. Note that these definitions
218 are slightly different than in Peng et al. (2016). All definitions of the types of conditions are summarized
219 in Table 3.

220 2.3 Uncertainty analysis

221 We apply the same method as in Peng et al. (2014, 2015) to calculate and analyze the output
222 uncertainties due to uncertain kinetic parameters in the model. Random samples following log-normal
223 distributions are generated for all rate constants and photoabsorption cross sections in the model using
224 uncertainty data available in the JPL database (Sander et al., 2011) or estimated based on IUPAC data
225 (Ammann et al., 2016). Then, Monte Carlo Uncertainty Propagation (BIPM et al., 2008) is performed for
226 these samples through the model to obtain the distributions of outputs. Finally, we compute squared
227 correlation coefficients between corresponding input and output samples and apportion the relative
228 contributions of individual kinetic parameters to the output uncertainties based on these coefficients

Deleted: risk

230 (Saltelli et al., 2005).

231 3 Results and discussion

232 In this section, we study the NO_y chemistry in OFR while considering relevant experimental issues.
233 Based on these results, we propose some guidelines for OFR operation for high-NO OH oxidation of
234 VOCs.

235 3.1 NO_y chemistry in typical OFR cases with initial NO injection

236 NO was thought to be unimportant (i.e., unable to significantly react with RO₂) in OFRs with initial
237 NO injection (OFR-iNO) based on the argument that its lifetime is too short due to large amounts of O₃
238 OH, and HO₂ to compete with RO₂+HO₂ (Li et al., 2015). We evaluate this issue below by calculating NO
239 effective lifetime (τ_{NO} , in s), defined as NO exposure (NO_{exp}, in molecules cm⁻³ s) divided by initial NO
240 concentration, under various conditions. This definition cannot effectively capture the true NO average
241 lifetime if it is close to or longer than the residence time. In this case, τ_{NO} close to the residence time
242 will be obtained, which is still long enough for our characterization purposes.

243 3.1.1 OFR185-iNO

244 In OFR185-iNO, NO is *not* oxidized extremely quickly under *all* conditions. For instance, under a
245 typical condition in the midrange of the phase space shown in Fig. 1a, $\tau_{NO} \sim 13$ s. This lifetime is much
246 shorter than the residence time, but long enough for OH_{exp} to reach $\sim 3 \times 10^{10}$ molecules cm⁻³ s, which is
247 equivalent to an OH equivalent age of ~ 6 hrs. Such an OH equivalent age is already sufficient to allow
248 some VOC processing and even SOA formation to occur (Lambe et al., 2011; Ortega et al., 2016). Within
249 τ_{NO} , NO suppresses HO₂ through the reaction $NO+HO_2 \rightarrow NO_2+OH$, leading to NO_{exp}/HO_{2exp} of ~ 700 during
250 this period, high enough for RO₂ to dominantly react with NO. Meanwhile, $NO+HO_2 \rightarrow NO_2+OH$ enhances
251 OH production, which helps OH_{exp} build up in a relatively short period. In addition, non-tropospheric
252 photolysis of VOCs at 185 and 254 nm is minor ($F_{185exp}/OH_{exp} \sim 600$ cm/s, Fig. 1a), because of enhanced
253 OH production and moderate UV. Therefore, such an OFR condition may be of some interest for high-
254 NO VOC oxidation. We thus analyze the NO_y chemistry in OFR185-iNO in more detail below, by taking
255 the case shown in Fig. 1a as a representative example.

256 In OFR185-iNO, HO_x concentrations are orders-of-magnitude higher than in the atmosphere
257 while the amount of O₃ produced is relatively small during the first several seconds after the flow enters
258 the reactor. As a result, NO is not oxidized almost exclusively by O₃ as in the troposphere, but also by
259 OH and HO₂ to form HONO and NO₂, respectively (Fig. 1a). The large concentration of OH present then
260 oxidizes HONO to NO₂, and NO₂ to HNO₃. Photolysis only plays a negligible role in the fate of HONO and
261 NO₂ in OFRs, in contrast to the troposphere, where it is the main fate of these species. This is because
262 the reactions of HONO and NO₂ with OH are greatly accelerated in OFR compared to those in the
263 troposphere, while photolysis not (Peng et al., 2016). The interconversion between NO₂ and HO₂NO₂ is
264 also greatly accelerated (Fig. 1a), since a large amount of HO₂ promotes the formation of HO₂NO₂,
265 whose thermal decomposition and reaction with OH in turn enhance the recycling of NO₂. Though not
266 explicitly modeled in this study, RO₂ are expected to undergo similar reactions with NO₂ to form
267 reservoir species, i.e., peroxy nitrates (Orlando and Tyndall, 2012). Peroxy nitrates that decompose on

Deleted: to suppress HO₂ through the reaction $NO+HO_2 \rightarrow NO_2+OH$, leading to NO_{exp}/HO_{2exp} of ~ 700 during this period, high enough

Deleted: RO₂ to dominantly react with NO. Meanwhile, $NO+HO_2 \rightarrow NO_2+OH$ enhances OH production. Within τ_{NO} ,

Deleted: reaches

Deleted: ,

Deleted: NO₂ and

Deleted: , respectively.

Deleted: is

Deleted: main atmospheric

Deleted: , but photolysis proceeds to a much smaller extent (typically orders of magnitude smaller in terms of e-fold decay)

Deleted: than

Deleted: at the same

Deleted: equivalent age

Deleted: However, the

284 timescales considerably longer than OFR residence times may serve as effectively permanent NO_y sinks
285 in OFRs (see Section 3.4.1).

Deleted: greater

Deleted: 3

286 Interestingly but not surprisingly, the NO_y chemistry shown in Fig. 1a is far from temporally
287 uniform during the OFR residence time (Fig. S1a). Within τ_{NO} , NO undergoes an e-fold decay as it is
288 rapidly converted into NO₂ and HONO, whose concentrations reach maxima around that time. After
289 most NO is consumed, HONO and NO₂ also start to decrease, but significantly more slowly than NO,
290 since they do not have as many and efficient loss pathways as NO. The reaction of OH with HONO, the
291 dominant fate of HONO, is slower than that with NO_x (Fig. 1a). The net rate of the NO₂-to-HO₂NO₂
292 conversion becomes low because of the relatively fast reverse reaction (Fig. 1a). Besides, the total loss
293 of NO₂ is partially offset by the production from HONO. The generally stable concentrations of HONO
294 and NO₂ (Fig. S1a) result in their respective reaction rates with OH that are comparable during and after
295 τ_{NO} (Fig. 1a), as OH variation is also relatively small during the entire residence time (Fig. S1b). However,
296 the NO₂-to-HO₂NO₂ conversion after τ_{NO} is much faster than during it (Fig. 1a), resulting from
297 substantially decreased NO and HO₂ concomitantly increasing >1 order of magnitude after τ_{NO} (Fig.
298 S1a,b). HNO₃ and HO₂NO₂, which are substantially produced only after NO₂ is built up, have much higher
299 concentrations later than within τ_{NO} .

Deleted: τ_{NO}

Deleted: .

Deleted: .

Deleted: τ_{NO} ,

Deleted: τ_{NO}

Deleted: ,

Deleted: τ_{NO}

Deleted: S1b

Deleted: τ_{NO}

300 Under other OFR185-iNO conditions than in Fig. 1a, the major reactions interconverting NO_y
301 species are generally the same, although their relative importance may vary. At lower NOⁱⁿ, the
302 perturbation of HO_x chemistry caused by NO_y species is smaller. Effects of NOⁱⁿ less than 1 ppb (e.g.,
303 typical non-urban ambient concentrations) are generally negligible regarding HO_x chemistry. Regarding
304 NO_y species, the pathways in Fig. 1a are still important under those conditions. At higher NOⁱⁿ (e.g., >1
305 ppm), one might expect NO₃ and N₂O₅ to play a role (as in OFR254-iNO; see Section 3.1.2 below), since
306 high NO_y concentrations might enhance self/cross reactions of NO_y. However, this would not occur
307 unless OH production is high, since relatively low O₃ concentrations in OFR185-iNO cannot oxidize NO₂
308 to NO₃ rapidly. Also, a large amount of NO_y can lead to significant OH suppression. That would in turn
309 slow down the NO₃ production from HNO₃ by OH. This is especially true when an OFR is used to oxidize
310 the output of highly concentrated sources (e.g., from vehicle exhausts). When sources corresponding
311 to OHR_{ext} of thousands of s⁻¹ and NOⁱⁿ of tens of ppm are injected into OFR185 (Fig. 1b), they essentially
312 inhibit active chemistry except NO consumption, as all subsequent products are much less abundant
313 compared to remaining NO (Fig. S1c).

314 3.1.2 OFR254-iNO

315 The ppm-level O_{3,in} used in the OFR254-iNO mode of operation has a strong impact on its NO_y
316 chemistry. An O_{3,in} of 2.2 ppm (lowest in this study) is already enough to shorten τ_{NO} to ~1 s, preventing
317 NO from playing a role in the chemistry under most explored conditions. The reaction fluxes under a
318 typical O_{3,in} of 7 ppm are shown in Fig. 1c. A reactive flux from NO+O₃→NO₂ makes the reaction of NO
319 with other oxidants (OH, HO₂ etc.) negligible. The HNO₃ production pathway from NO₂ is similar to that
320 in OFR185-iNO. The interconversion between NO₂ and HO₂NO₂ is also fast over the residence time, and
321 even faster than in OFR185-iNO during τ_{NO} , since a high concentration of O₃ also controls the OH-HO₂

333 interconversion and makes HO₂ more resilient against suppression due to high NO (Fig. S1f; Peng et al.,
334 2015). A major difference in the NO_y chemistry in OFR254-iNO (Fig. 1c) compared to OFR185-iNO (Fig.
335 1a) is significant NO₃/N₂O₅ chemistry due to high O₃ in OFR254-iNO, which accelerates the oxidation of
336 NO₂ to NO₃. Interconversion between NO₂+NO₃ and N₂O₅ also occurs to a significant extent because of
337 high NO₂. Under the conditions of Fig. 1c, NO₃ can also be significantly consumed by HO₂. Unlike
338 OFR185-iNO, OFR254-iNO can substantially form NO₃ from HNO₃ under conditions that are not on the
339 extremes of the explored physical condition space, e.g., at higher UV and lower NOⁱⁿ (e.g., Fig. S2). In
340 the case of very high NOⁱⁿ (equal to or higher than O_{3,in}), all O₃ can be rapidly destroyed by NO. As a
341 consequence, OH production is shut down and these cases are of little practical interest (Fig. S3h).

Deleted: .

342 3.1.3 Uncertainty analysis

343 The results of uncertainty propagation confirm that the output uncertainties due to uncertain
344 kinetic parameters are relatively low compared to other factors (e.g., non-plug flow in OFR; Peng et al.,
345 2015) and the overall model accuracy compared to experimental data (a factor of 2–3; Li et al., 2015).
346 For OFR185-iNO, NO, NO₃, and OH exposures have relative uncertainties of ~0–20%, ~40–70%, and ~15–
347 40%, respectively. The uncertainties in OH exposure are very similar to those in the cases without NO_x
348 (Peng et al., 2015). The contribution of NO_y reactions to OH_{exp} uncertainty is negligible, except for some
349 contribution of OH+NO→HONO in a few cases with high NOⁱⁿ (Fig. 2). The uncertainties on NO_{exp} are
350 dominated by the reactions producing HO_x and O₃, i.e., the major consumers of NO. For NO₃ exposure,
351 a few major production and loss pathways (e.g., NO₂+NO₃→N₂O₅, N₂O₅→NO₂+NO₃, and
352 HO₂+NO₃→OH+NO₂+O₂) dominate its uncertainties. OFR254-iNO has a simpler picture of parametric
353 uncertainties in terms of composition. O₃ controls the NO oxidation under most conditions and this
354 reaction contributes most of output uncertainties for NO exposures. HO₂+NO₃→OH+NO₂+O₂ dominates
355 the uncertainty on NO₃ exposure. The levels of those uncertainties are lower than in OFR185-iNO (<2%
356 for NO exposure; <60% in all cases and <25% in most cases for NO₃ exposure). Thus, model uncertainties
357 in OFR254-iNO are not shown in detail.

Deleted: with

358 3.2 Different conditions types

359 Having illustrated the main NO_y chemical pathways for typical cases, we present the results of
360 the exploration of the entire physical parameter space (see Section 2.2). Note that the explored space
361 is indeed very large and gridded logarithmically uniformly in every dimension. Therefore, the statistics
362 of the exploration results can be useful to determine the relative importance of the conditions types
363 defined in Section 2.2 and Table 3.

Deleted: of

364 It has been shown that during τ_{NO}, RO₂ can react dominantly with NO (Section 3.1.1), while to
365 determine if a condition is high-NO (see Table 3), the entire residence time is considered. This is done
366 because for VOC oxidation systems of interest, there will be significant oxidation of the initial VOC and
367 its products under low-NO conditions, if τ_{NO} is shorter than the reactor residence time. After most NO
368 is consumed, the longer the remaining residence time, the more RO₂ will react with HO₂ and the more
369 likely that an input condition is classified as low-NO. For a condition to be high-NO, a significantly long
370 τ_{NO} is required. [Figure 3 shows the fractional occurrence distribution of good/risky/bad conditions in](#)

374 the entire explored condition space over logarithm of $r(\text{RO}_2+\text{NO})/r(\text{RO}_2+\text{HO}_2)$, which distinguishes high-
375 and low-NO conditions. In OFR254-iNO, τ_{NO} is so short that no good high-NO condition is found in the
376 explored range in this study (Fig. 3a). A fraction of explored conditions are bad high-NO. These
377 conditions result from a full consumption of O_3 by NO. Then very little HO_x is produced, (right panels in
378 Fig. S3h), but the fate of any RO_2 formed is dominated by RO_2+NO , (right panels in Fig. S3i). However,
379 also due to negligibly low OH concentration, little RO_2 is produced and non-tropospheric photolysis of
380 VOCs is also substantial compared to their reaction with OH under these conditions, classifying all of
381 them as “bad” (Fig. 3a).

Deleted: ,

Deleted: .

Deleted: .”

382 In OFR185-iNO, in addition to the typical case shown in Fig. 1a, many other cases have a τ_{NO} of
383 ~ 10 s or longer (Figs. S3b and S4), which allow the possibility of high-NO conditions. Indeed, $\sim 1/3$ of
384 explored conditions in OFR185-iNO with a residence time of 3 min are high-NO (Fig. 3b). Most of these
385 high-NO conditions are also classified as bad, similar with those in OFR254-iNO. More importantly, in
386 contrast to OFR254-iNO, good and risky high-NO conditions also comprise an appreciable fraction of
387 the OFR185-iNO conditions. It is easily expected that very high OHR_{ext} and NO^{in} lead to bad high-NO
388 conditions (all panels in Fig. 4), since they strongly suppress HO_x , which yields bad conditions and in
389 turn keep NO destruction relatively low. Besides, the occurrence of bad high-NO conditions is reduced
390 at high UV, (bottom panels in Fig. 4), which can be explained by lowered NO due to high O_3 production
391 and fast OH reactant loss due to high OH production. Good high-NO conditions are rare in the explored
392 space. They are only 1.1% of total explored conditions (Fig. 3b) and present under very specific
393 conditions, i.e., higher H_2O , lower UV, lower OHR_{ext} , and NO^{in} of tens to hundreds of ppb (Figs. 4 and
394 S5). Since a very high NO can suppress OH, to obtain both a significant NO level and a good conditions,
395 NO^{in} can only be tens to hundreds of ppb. As NO^{in} is lower and OH is higher than under bad high-NO
396 conditions, UV should be lower than bad high-NO conditions to keep a sufficiently long presence of NO.
397 Thus, UV at 185 nm for good high-NO conditions are generally lower than 10^{12} photons $\text{cm}^{-2} \text{s}^{-1}$ (Fig. S5).
398 In addition, a low OHR_{ext} (generally $< 50 \text{ s}^{-1}$) and a higher H_2O (the higher the better, although there is
399 no apparent threshold) are also required for good high-NO conditions (Fig. S5), as Peng et al. (2016)
400 pointed out. Risky high-NO conditions often occur between good and bad high-NO conditions, e.g., at
401 lower NO^{in} than bad conditions (e.g., Cases ML, MM, HL, and HM in Fig. 4, see Table 2 for the typical
402 case label code), at higher OHR_{ext} and/or NO^{in} than good conditions (e.g., Cases ML and MM), and at
403 lower H_2O than good conditions (e.g., Case LL).

Deleted: ,

Deleted: at

Deleted: UV

Deleted: S4

Deleted: S4), which is also the UV criterion set for the good region in Peng et al. (2016).

Deleted: S4

404 The trend of the distributions of good, risky, and bad low-NO conditions is generally in line with
405 the analysis in Peng et al. (2016). For low-NO conditions, NO, species can be simply regarded as external
406 OH reactants, as in Peng et al. (2016). As H_2O decreases and/or OHR_{ext} or NO^{in} increases, a low-NO
407 condition becomes worse (good \rightarrow risky \rightarrow bad) (Figs. 4 and 5). In OFR185-iNO, increasing UV generally
408 makes a low-NO condition better because of an OH production enhancement (Fig. 4); while in OFR254-
409 iNO, increasing UV generally makes a low-NO condition worse (Fig. 5), since at a higher UV, more O_3 is
410 destroyed and the resilience of OH to suppression is reduced.

Deleted: did.

Deleted: ;

Deleted: ,

411 As discussed above, the fraction of high-NO conditions also depends on OFR residence time. A

426 shorter residence time is expected to generally lead to a larger fraction of high-NO conditions, since the
427 time spent in the reaction for $t > \tau_{NO}$ is significantly smaller. Thus, we also investigate an OFR185-iNO
428 case with a residence time of 30 s. In Fig. 3b, compared to the case with a residence time of 3 min, the
429 distributions of all condition types (good/risky/bad) of the 30 s residence time case shift toward higher
430 $r(\text{RO}_2+\text{NO})/r(\text{RO}_2+\text{HO}_2)$. Nevertheless, shortening the residence time also removes the period when the
431 condition is better (i.e., less non-tropospheric photolysis), when external OH reactants have been
432 partially consumed and OH suppression due to OHR_{ext} has been reduced later in the residence time. As
433 a result, the fractions of good and risky conditions decrease (Fig. 3b). With the two effects (higher
434 $r(\text{RO}_2+\text{NO})/r(\text{RO}_2+\text{HO}_2)$ and more significant non-tropospheric photolysis) combined, the fraction of
435 good high-NO conditions increases by a factor of ~ 3 . An even shorter residence time does not result in
436 a larger good high-NO fraction, since the effect of enhancing non-tropospheric photolysis is even more
437 apparent.

438 **3.3 Effect of non-plug flow**

439 We performed model runs where the only change with respect to our box model introduced in
440 Section 2.2 is that the plug-flow assumption is replaced by the residence time distribution (RTD)
441 measured by Lambe et al. (2011) (also see Fig. S8 of Peng et al. (2015)). The chemistry of different air
442 parcels with different residence times is simulated by our box model and outputs are averaged over the
443 RTD. Lateral diffusion between different air parcels is neglected in these simulations.

444 OH_{exp} calculated from the mode with RTD ($\text{OH}_{\text{exp,RTD}}$) is higher than that calculated from the plug-
445 flow model ($\text{OH}_{\text{exp,PF}}$) in both OFR185-iNO and OFR254-iNO (Table 4 and Fig. S6). Under most explored
446 conditions deviations are relatively small, which leads to an overall positive deviation of $\text{OH}_{\text{exp,RTD}}$ from
447 $\text{OH}_{\text{exp,PF}}$ by ~ 2 (within the uncertainties of the model and its application to real experimental systems).
448 For OFR185-iNO, most conditions ($\sim 90\%$) in the explored space lead to < 3 differences between $\text{OH}_{\text{exp,PF}}$
449 and $\text{OH}_{\text{exp,RTD}}$, while for a small fraction of cases the differences can be larger (Fig. S6). The larger
450 deviations are mainly present at high UV, OHR_{ext} , and NO^{in} , where conditions are generally “bad” and in
451 which experiments are of little atmospheric relevance. Under these specific conditions, external OH
452 reactants and NO_y can be substantially destroyed for the air parcels with residence times longer than
453 the average, while this is not the case for the average residence time. This feature was already described
454 by Peng et al. (2015) (see Fig. S10 of that study). Although only non- NO_y external OH reactants were
455 considered in that study, the results are the same. In the present study, a higher upper limit of the
456 explored OHR_{ext} range (compared to Peng et al., 2015, due to trying to simulate extremely high OHR_{ext}
457 used in some recent literature studies) large amounts of NO_y and cause somewhat larger deviations. In
458 OFR254-iNO, OH is less suppressed at high OHR_{ext} and NO^{in} than in OFR185-iNO because of high O_3
459 (Peng et al., 2015), $\text{OH}_{\text{exp,RTD}}$ deviations from $\text{OH}_{\text{exp,PF}}$ are also smaller (Table 4).

460 Based on the outputs of the model with RTD, similar mapping of the physical input space as Figs.
461 4 and 5 can be done (Figs. S7 and S8). Overall, the mapping of the RTD model results is very similar with
462 that of the plug-flow model. The conditions appear to be only slightly better in a few places of the
463 explored space than those from the plug-flow model, which can be easily explained by the discussions

Deleted: .

465 above. Besides, the mapping in Figs. S7 and S8 also appear to be slightly more low-NO, for the same
466 reasons discussed above. After NO is destroyed at long residence times, HO₂, suppressed by NO, also
467 recovers as OH. $r(\text{RO}_2+\text{NO})/r(\text{RO}_2+\text{HO}_2)$ is obviously expected to be smaller than in the plug-flow model
468 in general.

469 Note that most conditions that appear to be better in the RTD model results are already
470 identified as bad by the plug-flow model. Those conditions look slightly better only because of their
471 better RTD-averaged $F_{185_{\text{exp}}}/\text{OH}_{\text{exp}}$ and $F_{254_{\text{exp}}}/\text{OH}_{\text{exp}}$. However, each of those cases is actually
472 composed of both a better part at longer residence times and also a worse part at shorter residence
473 times. Under those conditions, the reactor simultaneously works in two distinct regimes, one of which
474 is bad due to heavy OH suppression. Such conditions are obviously not desirable for OFR operation.

475 **3.4 Possible issues related to high-NO_x levels**

476 In the discussion above, we focused on obtaining high-NO conditions and considered only one
477 experimental issue (non-tropospheric photolysis) that had been previously investigated in Peng et al.
478 (2016) and is not specific for experiments with high NO injection. We discuss additional potential
479 reasons why the OFR-iNO chemistry can deviate strongly from tropospheric conditions, as specifically
480 related to high-NO_x level in this subsection.

481 **3.4.1 NO₂**

482 NO₂ reacts with RO₂ to form peroxy nitrates, generally regarded as reservoir species in the
483 atmosphere as most of them thermally decompose very quickly compared to atmospheric time scales.
484 However, in OFRs, with residence times on the order of minutes, some peroxy nitrates may no longer be
485 considered as fast decomposing. This is especially true for acylperoxy nitrates, whose lifetimes can be
486 hours at room temperature (Orlando and Tyndall, 2012). Acylperoxy nitrates are essentially sinks instead
487 of reservoirs in OFRs for both NO₂ and RO₂. RO₂ is estimated to be as high as several ppb in OFRs by our
488 model (e.g., ~6 ppb RO₂ in OFR185 at H₂O=1%, UV at 185 nm=1x10¹³ photons cm⁻² s⁻¹, OHR_{exit}=1000 s⁻¹,
489 and NO⁰=0), while high-NO experiments can yield far higher NO₂. If all RO₂ were acylperoxy, the RO₂
490 chemistry could be rapidly shut down by NO₂, as rate constants of these RO₂ + NO₂ reactions are around
491 10⁻¹¹ cm³ molecule⁻¹ s⁻¹ (Orlando and Tyndall, 2012). Nevertheless, acylperoxy nitrates are not expected
492 to typically be the dominant component of peroxy nitrates, since acyl radicals are not a direct oxidation
493 product of most common VOCs and can only be formed after several steps of oxidation (Atkinson and
494 Arey, 2003; Ziemann and Atkinson, 2012). Most alkylperoxy nitrates retain their short-lived reservoir
495 characteristics in OFRs due to their relatively short thermal decomposition time scales (on the order of
496 0.1 s; Orlando and Tyndall, 2012). Even so, OFR experiments can be seriously hampered at extremely
497 high NO₂. If NO₂ reaches ppm levels, the equilibrium between RO₂+NO₂ and alkylperoxy nitrate
498 (RO₂+NO₂↔RO₂NO₂) is greatly shifted toward the alkylperoxy nitrate side, as the forward and reverse
499 rate constants are on the order of 10⁻¹² cm³ molecule⁻¹ s⁻¹ and 1 s⁻¹, respectively (Orlando and Tyndall,
500 2012). This results in a substantial decrease in effective RO₂ concentration, or in other words, a
501 substantial slow-down of RO₂ chemistry.

502 Parts per million levels of NO₂ may impose an additional experimental artifact in the oxidation

503 chemistry of aromatic precursors. OH-aromatic adducts, i.e., the immediate products of aromatic
504 oxidation by OH, undergo addition of O₂ and NO₂ at comparable rates under ppm levels of NO₂ (rate
505 constants of the additions of O₂ and NO₂ are on the order of 10⁻¹⁶ and 10⁻¹¹ molecules cm⁻³ s⁻¹,
506 respectively ;Atkinson and Arey, 2003). However, only the former addition is atmospherically relevant
507 (Calvert et al., 2002). Liu et al. (2015) performed OFR254-iNO experiments with toluene over a range of
508 NOⁱⁿ of 2.5–10 ppm, encompassing the NO concentration range at which the reactions of OH-toluene
509 adduct with O₂ and with NO₂ are of equal importance (~5 ppm; Atkinson and Arey, 2003). This suggests
510 that nitroaromatics, whose formation was reported in the study of Liu et al. (2015), might have been
511 formed in substantial amounts in that study through the addition of NO₂ to the OH-toluene adduct.

512 3.4.2 NO₃

513 As discussed in Section 3.1, NO₃ can be formed in significant amounts in OFRs with high NO
514 injection. Although NO₃ is also present in the atmosphere, especially during nighttime, significant VOC
515 oxidation by both OH and NO₃ results in more complex chemistry that may complicate the
516 interpretation of experimental results. NO₃ oxidation-only OFR has been previously realized
517 experimentally via thermal dissociation of injected N₂O₅ (Palm et al., 2017). We discuss below how to
518 avoid significant VOC oxidation by NO₃ and achieve OH-dominated VOC oxidation in OFRs with high NO
519 injection.

520 If NO_{3exp}/OH_{exp} > 0.1, NO₃ can be a competitive reactant for biogenic alkenes and dihydrofurans,
521 which have a C=C bond for NO₃ addition, and phenols, which have activated hydroxyl for fast hydrogen
522 abstraction by NO₃ (Atkinson and Arey, 2003), while for lower NO_{3exp}/OH_{exp}, OH is expected to dominate
523 the oxidation of all VOCs, as shown in Fig. 6. Oxidation for VOCs without alkene C=C bonds and phenol
524 hydroxyl (such as alkanes and (alkyl)benzenes) is dominated by OH unless NO_{3exp}/OH_{exp} > 1000. Despite
525 its double bond, ethene reacts as slowly with NO₃ as alkanes, likely due to lack of alkyl groups enriching
526 electron density on the C=C bond, which slows NO₃ addition. We calculate NO_{3exp}/OH_{exp} for OFR185-
527 iNO and OFR254-iNO and plot histograms of this ratio in Fig. 6. Many experimental conditions lead to
528 high enough NO_{3exp}/OH_{exp} that NO₃ is a competitive sink for alkenes, while only under very extreme
529 conditions can NO₃ be a competitive sink for species without C=C bonds. High-NO conditions in OFR185-
530 iNO have lower NO_{3exp}/OH_{exp} (~10⁻²–10²) than in OFR254-iNO (~10¹–10⁵) (Figs. 6 and S3d,g,i). This
531 difference in NO_{3exp}/OH_{exp} is due to the different levels of O₃ in the two modes, as high O₃ promotes
532 NO₂-to-NO₃ oxidation. Note that low-NO conditions in both OFR185-iNO and OFR254-iNO can also reach
533 high NO_{3exp}/OH_{exp} as some high-NO conditions have. This is because in OFR185-iNO a large part of NO₃
534 is formed by OH oxidation, resulting in NO_{3exp}/OH_{exp} being largely influenced by NOⁱⁿ but not by other
535 factors mainly governing OH, (Fig. S3d); and under low-NO conditions in OFR254-iNO, NO₃ can form
536 rapidly from NO₂+O₃, while OH can be heavily suppressed by high OHR_{ext} (Fig. S3g,i).

537 Most of the species shown in Fig. 6 are primary VOCs, except phenols and a dihydrofuran, which
538 can be intermediates of the atmospheric oxidation of (alkyl)benzenes (Atkinson and Arey, 2003) and
539 long-chain alkanes (Aimanant and Ziemann, 2013; Strollo and Ziemann, 2013; Ranney and Ziemann,
540 2016), respectively. Nevertheless, only the phenol production may occur in high-NO OFRs, as the

Deleted: .

Deleted: ;

Deleted: .

544 particle-phase reaction in the photochemical formation of dihydrofurans from alkanes is too slow
545 compared to typical OFR residence times (Ranney and Ziemann, 2016). Therefore, the impact of NO₃
546 oxidation on VOC fate needs to be considered only if the OFR input flow contains high NO mixed with
547 biogenics and/or aromatics [(alkyl)benzenes and/or phenols]. However, (alkyl)benzenes were likely to
548 be major SOA precursors in, to our knowledge, the only few literature OFR studies with high NO levels
549 (Ortega et al., 2013; Tkacik et al., 2014; Liu et al., 2015). In the study of the air in a traffic tunnel (OFR185-
550 iNO mode; Tkacik et al., 2014), where toluene is usually a major anthropogenic SOA precursor as in
551 other urban environments (Dzepina et al., 2009; Borbon et al., 2013; Hayes et al., 2015; Jathar et al.,
552 2015), NO_x was several hundreds of ppb. This resulted in an estimated NO_{3exp}/OH_{exp} range of ~0.1–1,
553 where up to ~30% of cresols (intermediates of toluene oxidation) may have been consumed by NO₃.
554 Dihydrofurans may also have formed in the tunnel air (but outside the OFR) in the presence of NO_x
555 (Aimanant and Ziemann, 2013; Strollo and Ziemann, 2013) and, after entering the OFR, they would have
556 been substantially (up to ~50%) consumed by NO₃. In the laboratory experiment of Liu et al. (2015) with
557 toluene, the injection of as much as 10 ppm NO elevated NO_{3exp}/OH_{exp} to ~100, where cresols from
558 toluene oxidation reacted almost exclusively with NO₃ in addition to being photolyzed.

559 3.4.3 A case study

560 We use a case study of an OFR254-13-iNO laboratory experiment with a large amount of toluene
561 (5 ppm) and NOⁱⁿ (10 ppm) to illustrate how very high VOC and NO concentrations cause multiple types
562 of atmospherically irrelevant reactions in OFR. Due to very high OHR_{ext} and NOⁱⁿ, photolysis of toluene
563 at 254 nm may have been important (Peng et al., 2016). In case of a high (close to 1) quantum yield, up
564 to ~80% of the consumed toluene in their experiments could have been photolyzed (Scheme 1). Of the
565 rest of reacted toluene, ~10% undergoes H-abstraction by OH from the methyl group in the model,
566 leading to an RO₂ similar to alkyl RO₂ and likely proceeding with normal RO₂ chemistry. ~90% of the
567 toluene formed an OH-adduct (Calvert et al., 2002). As discussed above, 70% of this adduct (depending
568 on NOⁱⁿ) is predicted to recombine with NO₂ producing nitroaromatics because of the ppm-level NO_x.
569 The adduct could also react with O₂ via two types of pathways, of which one was addition forming a
570 special category of RO₂ (OH-toluene-O₂ adducts) potentially undergoing ring-opening (Atkinson and
571 Arey, 2003; Orlando and Tyndall, 2012; Ziemann and Atkinson, 2012), the other H-elimination by O₂
572 producing cresols. Again, like toluene, cresols may have been substantially photolyzed. As a result of
573 NO_{3exp}/OH_{exp} ~100, only a minor portion of cresol could have undergone OH₂ addition and then H-
574 elimination again. This pathway leads to the formation of methylidihydroxybenzenes and other OH-
575 oxidation products (Atkinson and Arey, 2003). The rest of cresols may have formed methylphenoxy
576 radicals, nevertheless, dominantly via H-abstraction by NO₃, since H-abstraction by OH was even a minor
577 pathway compared to the OH-addition one (Atkinson et al., 1992). In summary, the model results
578 suggest that there were two possible routes leading to nitroaromatic formation. However, one of them
579 (recombination of OH-aromatic adducts with NO₂) is likely of little atmospheric relevance due to very
580 high NO_x, needed, and the other (H-abstraction from cresol) occurs in the atmosphere but is not a major
581 fate of aromatics (Calvert et al., 2002).

Deleted: cresols

Deleted: repeated

Deleted: -

Deleted: -

Deleted: process forming

Deleted: was

588 **3.5 Implications for OFR experiments with combustion emissions as input**

589 Emissions from combustion sources, e.g., vehicles and biomass burning, usually contain VOCs
590 and NO_x at very high concentrations (Table 1). An injection of this type of emissions (typically with OHR_{ext}
591 of thousands of s⁻¹ or larger and NOⁿ of tens of ppm or larger) in OFRs without any pretreatment is likely
592 to cause all experimental issues discussed in Peng et al. (2016) and this paper, i.e., strong OH
593 suppression, substantial non-tropospheric photolysis, strong RO₂ suppression by NO₂ whether RO₂ is
594 acyl RO₂ or not, fast reactions of NO₂ with OH-aromatic hydrocarbon adducts, substantial NO₃
595 contribution to VOC fate, and even a near-total inhibition of OFR chemistry due to complete titration of
596 O₃ by NO in the case of OFR254. We take the study of Karjalainen et al. (2016), who used an OFR to
597 oxidize diluted car exhaust in real-time, as a case study to investigate the extent to which these issues
598 may affect typical combustion source studies and to explore approaches to mitigate the problems.

599 During the first 200 s of their experiment (defined as the “cold start” period when the catalyst is
600 cold and emissions are high), NO and total hydrocarbon in the emissions of the test vehicle reached
601 ~400 and ~600 ppm, respectively. We first simulate the oxidation of those emissions without any
602 dilution (even though x12 dilution was used in their experiments) to explore the most extreme
603 conditions. Our model simulation indicates that such an extremely concentrated source would generally
604 lead to bad high- or low-NO conditions (depending on NO concentration) in their OFR (Fig. 7), even
605 though it was run at relatively high H₂O and UV. OH suppression can be as high as 3 orders of magnitude;
606 VOC fates by non-tropospheric photolysis and reactions of alkenes and phenols with NO₃ can be nearly
607 100%; up to ~1/3 of OH-toluene adduct may be recombined with NO₂ instead of forming an adduct with
608 O₂. After the test vehicle entered the “hot stabilized” stage (200–1000 s), its VOC emissions (on the
609 order of ppm) were still too high for an undiluted OFR to yield a good condition (Fig. S9). OH suppression
610 can still reach 2 orders of magnitude; non-tropospheric photolysis, and sometimes reactions with NO₃,
611 can still dominate over reactions with OH in VOC fates; reactions of OH-toluene adduct with NO₂ can
612 still be substantial at some small NO emission spikes. Moreover, although NO emissions were roughly
613 at ppm level even during the hot stabilized period, NO effective lifetime may be very short during that
614 period, leading to low-NO conditions in their OFR.

615 As suggested in Peng et al. (2016) for low-NO OFR, dilution of sources can also mitigate strong
616 deviations on OFR-iNO chemistry vs. atmospherically-relevant conditions. A dilution by a factor of 12,
617 as actually used by Karjalainen et al. (2016), appears to be sufficient to bring most of the hot stabilized
618 period under good conditions (Fig. S9). However, most VOC, or in other words, most SOA formation
619 potential, was emitted during the cold start period, when risky and bad conditions still prevailed (Figs.
620 7 and 8). Even if the emissions are diluted by x100, the cold-start emission peak (Fig. 7) is still under
621 risky conditions. Although bad conditions are eliminated and good condition is present during most of
622 time, this emission peak under risky condition may contribute >50% to total SOA formation potential
623 (Fig. 8). For SOA formed under good condition to be dominant, a dilution factor >400 would be needed.

624 Note that the emissions of the test vehicle of Karjalainen et al. (2016) are rather clean compared
625 to the typical 2013 US on-road fleet (i.e., all at the hot stabilized stage) measured by Bishop and

Deleted: S5

Deleted: S5

628 Stedman (2013) (Figs. 9 and §10). For emissions of an average on-road fleet, a dilution by a factor of
629 100 or larger would be necessary to ensure that most emissions would be processed in OFR185 under
630 good conditions at the highest H₂O and UV in this study (Figs. 9b and §10b,e,h). In the case of lower H₂O
631 and/or UV, an even larger dilution factor would be required.

Deleted: S6

Deleted: S6b

632 Conducting OFR185-iNO experiments at high UV lowers the dilution factor needed for good
633 conditions. However, it also renders good high-NO condition impossible (see Section 3.2 and Fig. S4). If
634 one wants to oxidize vehicle exhausts in a high-NO environment in OFR, as in an urban atmosphere,
635 OFR185 at low UV is necessary. Consequently, a much stronger dilution is in turn necessary to keep the
636 operation condition still good. Nevertheless, not all vehicle emissions can be moved into good high-NO
637 region through a simple dilution (Figs. 9c and §10c,f,i). Furthermore, a low UV would seriously limit the
638 highest OH_{exp} that OFR can achieve (~3x10¹¹ molecules cm⁻³ s for modeled good high-NO conditions in
639 this study), while a much higher OH_{exp} would be desirable to fully convert SOA formation potential into
640 measurable SOA mass. If both good high-NO condition and high OH_{exp} are required, new techniques
641 (e.g., injection of N₂O at percent level proposed by Lambe et al. (2017)) may be necessary.

Deleted: S6c

642 4 Conclusions

643 In this study, OFR chemistry involving NO_y species was systematically investigated over a wide
644 range of conditions. NO initially injected into the OFR was found to be rapidly oxidized under most
645 conditions. In particular, due to high O₃ concentrations, NO lifetime in OFR254-iNO was too short to
646 result in a significant RO₂ consumption by NO compared to that by HO₂ under all conditions with active
647 chemistry. Nevertheless, it is not completely impossible for OFR185-iNO to have a significant RO₂ fate
648 by NO and minor non-tropospheric photolysis at the same time ("good high-NO conditions"). According
649 to our simulations, these conditions are most likely present at high H₂O, low UV, low OHR_{ext}, and NOⁿ
650 of tens to hundreds of ppb.

651 However, many past OFR studies with high NO injection were conducted under conditions
652 remarkably different from the abovementioned very narrow range. NOⁿ and/or OHR_{ext} in those studies
653 were often much higher than good high-NO conditions require (particularly, >3 orders of magnitude in
654 some OFR studies using combustion emissions as input). In addition to non-tropospheric organic
655 photolysis, OFR oxidation of highly concentrated sources can cause multiple large deviations from
656 tropospheric OH oxidation, i.e., RO₂ suppression by high NO₂, substantial nitroaromatic formation from
657 the recombination of NO₂ and OH-aromatic adducts, and fast reactions of VOCs with NO₃ compared to
658 those with OH.

659 Working at lower NO_x (sub-ppm level) and VOC concentrations or dilution can mitigate these
660 experimental problems. In general, a strong dilution (by a factor of >100) is needed for OFR that process
661 typical on-road vehicle emissions. Humidification can also make good conditions more likely. By these
662 measures, good conditions can be guaranteed, as long as NO and/or precursor concentrations are
663 sufficiently low, while high-NO conditions cannot be ensured. To aid design and interpretation of OFR
664 experiments with high NO injection, we provide our detailed modeling results in a visualized form (Fig.
665 §3). For OFR users in need for both high OH_{exp} and high NO, simple NO injection is not a good option.

Deleted: S7

670 New techniques (e.g., injection of N₂O proposed by Lambe et al. (2017) or other innovations) may be
671 necessary to meet this need.

672

673

674 **Acknowledgements**

675 This work was partially supported by DOE (BER/ASR) DE-SC0011105 & DE-SC0016559, EPA STAR
676 83587701-0, and NSF AGS-1360834. We thank Pengfei Liu, Andrew Lambe, and Daniel Tkacik for
677 providing some OFR experimental data, the authors of Karjalainen et al. (2016) and their project IEA-
678 AMF Annex 44 for providing the data and information for the vehicle tests, Gary Bishop for providing
679 on-road vehicle emission data, and Andrew Lambe and William Brune for useful discussions.
680

681 **References**

- 682 Aimanant, S. and Ziemann, P. J.: Chemical Mechanisms of Aging of Aerosol Formed from the Reaction
683 of n-Pentadecane with OH Radicals in the Presence of NO_x, *Aerosol Sci. Technol.*, 47(9), 979–990,
684 doi:10.1080/02786826.2013.804621, 2013.
- 685 Alanen, J., Simonen, P., Saarikoski, S., Timonen, H., Kangasniemi, O., Saukko, E., Hillamo, R., Lehtoranta,
686 K., Murtonen, T., Vesala, H., Keskinen, J. and Rönkkö, T.: Comparison of primary and secondary particle
687 formation from natural gas engine exhaust and of their volatility characteristics, *Atmos. Chem. Phys.*
688 *Discuss.*, (February), 1–27, doi:10.5194/acp-2017-44, 2017.
- 689 Ammann, M., Cox, R. A., Crowley, J. N., Jenkin, M. E., Mellouki, A., Rossi, M. J., Troe, J., Wallington, T. J.,
690 Cox, B., Atkinson, R., Baulch, D. L. and Kerr, J. A.: IUPAC Task Group on Atmospheric Chemical Kinetic
691 Data Evaluation, [online] Available from: <http://iupac.pole-ether.fr/#>, 2016.
- 692 Atkinson, R. and Arey, J.: Atmospheric degradation of volatile organic compounds., *Chem. Rev.*, 103(12),
693 4605–38, doi:10.1021/cr0206420, 2003.
- 694 Atkinson, R., Aschmann, S. M. and Arey, J.: Reactions of hydroxyl and nitrogen trioxide radicals with
695 phenol, cresols, and 2-nitrophenol at 296 ± 2 K, *Environ. Sci. Technol.*, 26(7), 1397–1403,
696 doi:10.1021/es00031a018, 1992.
- 697 BIPM, IEC, IFCC, ILAC, ISO, IUPAC and IUPAPOIML: JCGM 101: 2008 Evaluation of measurement data —
698 Supplement 1 to the “ Guide to the expression of uncertainty in measurement ” — Propagation of
699 distributions using a Monte Carlo method., 2008.
- 700 Bishop, G. A. and Stedman, D. H.: Fuel Efficiency Automobile Test: Light-Duty Vehicles, [online] Available
701 from: http://www.feat.biochem.du.edu/light_duty_vehicles.html (Accessed 1 February 2017), 2013.
- 702 Borbon, A., Gilman, J. B., Kuster, W. C., Grand, N., Chevaillier, S., Colomb, A., Dolgorouky, C., Gros, V.,
703 Lopez, M., Sarda-Esteve, R., Holloway, J., Stutz, J., Petetin, H., McKeen, S., Beekmann, M., Warneke, C.,
704 Parrish, D. D. and De Gouw, J. A.: Emission ratios of anthropogenic volatile organic compounds in
705 northern mid-latitude megacities: Observations versus emission inventories in Los Angeles and Paris, *J.*
706 *Geophys. Res. Atmos.*, 118(4), 2041–2057, doi:10.1002/jgrd.50059, 2013.
- 707 Burkholder, J. B., Sander, S. P., Abbatt, J., Barker, J. R., Huie, R. E., Kolb, C. E., Kurylo, M. J., Orkin, V. L.,
708 Wilmouth, D. M. and Wine, P. H.: Chemical Kinetics and Photochemical Data for Use in Atmospheric
709 Studies: Evaluation Number 18, Pasadena, CA, USA. [online] Available from:
710 <http://jpldataeval.jpl.nasa.gov/>, 2015.
- 711 Calvert, J. G., Atkinson, R., Becker, K. H., Kamens, R. M., Seinfeld, J. H., Wallington, T. H. and Yarwood,
712 G.: The Mechanisms of Atmospheric Oxidation of the Aromatic Hydrocarbons, Oxford University Press,
713 USA. [online] Available from: <https://books.google.com/books?id=P0basaLrxDMC>, 2002.
- 714 Carlton, A. G., Wiedinmyer, C. and Kroll, J. H.: A review of Secondary Organic Aerosol (SOA) formation
715 from isoprene, *Atmos. Chem. Phys.*, 9(14), 4987–5005, doi:10.5194/acp-9-4987-2009, 2009.
- 716 Carter, W. P. L., Cocker, D. R., Fitz, D. R., Malkina, I. L., Bumiller, K., Sauer, C. G., Pisano, J. T., Bufalino, C.
717 and Song, C.: A new environmental chamber for evaluation of gas-phase chemical mechanisms and
718 secondary aerosol formation, *Atmos. Environ.*, 39(40), 7768–7788,
719 doi:10.1016/j.atmosenv.2005.08.040, 2005.
- 720 Chameides, W., Lindsay, R., Richardson, J. and Kiang, C.: The role of biogenic hydrocarbons in urban
721 photochemical smog: Atlanta as a case study, *Science* (80-.), 241(4872), 1473–1475,
722 doi:10.1126/science.3420404, 1988.
- 723 Cocker, D. R., Flagan, R. C. and Seinfeld, J. H.: State-of-the-Art Chamber Facility for Studying Atmospheric
724 Aerosol Chemistry, *Environ. Sci. Technol.*, 35(12), 2594–2601, doi:10.1021/es0019169, 2001.
- 725 [Donahue, N. M., Posner, L. N., Westervelt, D. M., Li, Z., Shrivastava, M., Presto, A. A., Sullivan, R. C.,](#)
726 [Adams, P. J., Pandis, S. N. and Robinson, A. L.: Where Did This Particle Come From? Sources of Particle](#)
727 [Number and Mass for Human Exposure Estimates, in Airborne Particulate Matter: Sources, Atmospheric](#)
728 [Processes and Health, edited by R. M. Harrison, R. E. Hester, and X. Querol, pp. 35–71, Royal Society of](#)
729 [Chemistry, 2016.](#)
- 730 Dzepina, K., Volkamer, R. M., Madronich, S., Tulet, P., Ulbrich, I. M., Zhang, Q., Cappa, C. D., Ziemann, P.

731 J. and Jimenez, J. L.: Evaluation of recently-proposed secondary organic aerosol models for a case study
732 in Mexico City, *Atmos. Chem. Phys.*, 9(15), 5681–5709, doi:10.5194/acp-9-5681-2009, 2009.

733 George, I. J., Vlasenko, A., Slowik, J. G., Broekhuizen, K. and Abbatt, J. P. D.: Heterogeneous oxidation of
734 saturated organic aerosols by hydroxyl radicals: uptake kinetics, condensed-phase products, and particle
735 size change, *Atmos. Chem. Phys.*, 7(16), 4187–4201, doi:10.5194/acp-7-4187-2007, 2007.

736 Haagen-Smit, A. J.: Chemistry and Physiology of Los Angeles Smog, *Ind. Eng. Chem.*, 44(6), 1342–1346,
737 doi:10.1021/ie50510a045, 1952.

738 Hallquist, M., Wenger, J. C., Baltensperger, U., Rudich, Y., Simpson, D., Claeys, M., Dommen, J., Donahue,
739 N. M., George, C., Goldstein, A. H., Hamilton, J. F., Herrmann, H., Hoffmann, T., Iinuma, Y., Jang, M.,
740 Jenkin, M. E., Jimenez, J. L., Kiendler-Scharr, A., Maenhaut, W., McFiggans, G., Mentel, T. F., Monod, A.,
741 Prevot, A. S. H., Seinfeld, J. H., Surratt, J. D., Szmigielski, R. and Wildt, J.: The formation, properties and
742 impact of secondary organic aerosol: current and emerging issues, *Atmos. Chem. Phys.*, 9(14), 5155–
743 5236, 2009.

744 Hayes, P. L., Carlton, a. G., Baker, K. R., Ahmadov, R., Washenfelder, R. a., Alvarez, S., Rappenglück, B.,
745 Gilman, J. B., Kuster, W. C., de Gouw, J. a., Zotter, P., Prévôt, a. S. H., Szidat, S., Kleindienst, T. E., Offenberg,
746 J. H., Ma, P. K. and Jimenez, J. L.: Modeling the formation and aging of secondary organic aerosols in Los
747 Angeles during CalNex 2010, *Atmos. Chem. Phys.*, 15(10), 5773–5801, doi:10.5194/acp-15-5773-2015,
748 2015.

749 [Hearn, J. D. and Smith, G. D.: Kinetics and Product Studies for Ozonolysis Reactions of Organic Particles
750 Using Aerosol CIMS †, *J. Phys. Chem. A*, 108\(45\), 10019–10029, doi:10.1021/jp0404145, 2004.](#)

751 Hoffmann, T., Odum, J. R., Bowman, F., Collins, D., Klockow, D., Flagan, R. C. and Seinfeld, J. H.:
752 Formation of Organic Aerosols from the Oxidation of Biogenic Hydrocarbons, *J. Atmos. Chem.*, 26(2),
753 189–222, doi:10.1023/A:1005734301837, 1997.

754 [Hu, W., Palm, B. B., Day, D. A., Campuzano-Jost, P., Krechmer, J. E., Peng, Z., de Sá, S. S., Martin, S. T.,
755 Alexander, M. L., Baumann, K., Hacker, L., Kiendler-Scharr, A., Koss, A. R., de Gouw, J. A., Goldstein, A.
756 H., Seco, R., Sjostedt, S. J., Park, J.-H., Guenther, A. B., Kim, S., Canonaco, F., Prévôt, A. S. H., Brune, W.
757 H. and Jimenez, J. L.: Volatility and lifetime against OH heterogeneous reaction of ambient isoprene-
758 epoxydiols-derived secondary organic aerosol \(IEPOX-SOA\), *Atmos. Chem. Phys.*, 16\(18\), 11563–11580,
759 doi:10.5194/acp-16-11563-2016, 2016.](#)

760 Jathar, S. H., Cappa, C. D., Wexler, a. S., Seinfeld, J. H. and Kleeman, M. J.: Multi-generational oxidation
761 model to simulate secondary organic aerosol in a 3-D air quality model, *Geosci. Model Dev.*, 8(8), 2553–
762 2567, doi:10.5194/gmd-8-2553-2015, 2015.

763 Kang, E., Root, M. J., Toohey, D. W. and Brune, W. H.: Introducing the concept of Potential Aerosol Mass
764 (PAM), *Atmos. Chem. Phys.*, 7(22), 5727–5744, doi:10.5194/acp-7-5727-2007, 2007.

765 Kang, E., Toohey, D. W. and Brune, W. H.: Dependence of SOA oxidation on organic aerosol mass
766 concentration and OH exposure: experimental PAM chamber studies, *Atmos. Chem. Phys.*, 11(4), 1837–
767 1852, doi:10.5194/acp-11-1837-2011, 2011.

768 Karjalainen, P., Timonen, H., Saukko, E., Kuuluvainen, H., Saarikoski, S., Aakko-Saksa, P., Murtonen, T.,
769 Bloss, M., Dal Maso, M., Simonen, P., Ahlberg, E., Svenningsson, B., Brune, W. H., Hillamo, R., Keskinen,
770 J. and Rönkkö, T.: Time-resolved characterization of primary particle emissions and secondary particle
771 formation from a modern gasoline passenger car, *Atmos. Chem. Phys.*, 16(13), 8559–8570,
772 doi:10.5194/acp-16-8559-2016, 2016.

773 Krechmer, J. E., Pagonis, D., Ziemann, P. J. and Jimenez, J. L.: Quantification of Gas-Wall Partitioning in
774 Teflon Environmental Chambers Using Rapid Bursts of Low-Volatility Oxidized Species Generated in Situ,
775 *Environ. Sci. Technol.*, 50(11), 5757–5765, doi:10.1021/acs.est.6b00606, 2016.

776 [Lakey, P. S. J., George, I. J., Whalley, L. K., Baeza-Romero, M. T. and Heard, D. E.: Measurements of the
777 HO₂ Uptake Coefficients onto Single Component Organic Aerosols, *Environ. Sci. Technol.*, 49\(8\), 4878–
778 4885, doi:10.1021/acs.est.5b00948, 2015.](#)

779 Lambe, A., Massoli, P., Zhang, X., Canagaratna, M., Nowak, J., Daube, C., Yan, C., Nie, W., Onasch, T.,
780 Jayne, J., Kolb, C., Davidovits, P., Worsnop, D. and Brune, W.: Controlled nitric oxide production via
781 O(¹S) + N₂O → NO + O₂

Deleted:)+

783 reactions for use in oxidation flow reactor studies, *Atmos. Meas. Tech.*, **10**(6), 2283–2298,
784 doi:10.5194/amt-10-2283-2017, 2017.

785 Lambe, A. T., Ahern, A. T., Williams, L. R., Slowik, J. G., Wong, J. P. S., Abbatt, J. P. D., Brune, W. H., Ng, N.
786 L., Wright, J. P., Croasdale, D. R., Worsnop, D. R., Davidovits, P. and Onasch, T. B.: Characterization of
787 aerosol photooxidation flow reactors: heterogeneous oxidation, secondary organic aerosol formation
788 and cloud condensation nuclei activity measurements, *Atmos. Meas. Tech.*, **4**(3), 445–461,
789 doi:10.5194/amt-4-445-2011, 2011.

790 Lambe, A. T. and Jimenez, J. L.: PAM Wiki: Publications Using the PAM Oxidation Flow Reactor, [online]
791 Available from: <https://sites.google.com/site/pamwiki/publications> (Accessed 10 February 2017), 2017.

792 Levy II, H.: Normal atmosphere: large radical and formaldehyde concentrations predicted., *Science*,
793 **173**(3992), 141–143, doi:10.1126/science.173.3992.141, 1971.

794 Li, R., Palm, B. B., Borbon, A., Graus, M., Warneke, C., Ortega, a M., Day, D. a, Brune, W. H., Jimenez, J.
795 L. and de Gouw, J. a: Laboratory Studies on Secondary Organic Aerosol Formation from Crude Oil Vapors,
796 *Environ. Sci. Technol.*, **47**(21), 12566–12574, doi:10.1021/es402265y, 2013.

797 Li, R., Palm, B. B., Ortega, A. M., Hu, W., Peng, Z., Day, D. A., Knote, C., Brune, W. H., de Gouw, J. and
798 Jimenez, J. L.: Modeling the radical chemistry in an Oxidation Flow Reactor (OFR): radical formation and
799 recycling, sensitivities, and OH exposure estimation equation, *J. Phys. Chem. A*, **119**(19), 4418–4432,
800 doi:10.1021/jp509534k, 2015.

801 Link, M. F., Friedman, B., Fulgham, R., Brophy, P., Galang, A., Jathar, S. H., Veres, P., Roberts, J. M. and
802 Farmer, D. K.: Photochemical processing of diesel fuel emissions as a large secondary source of isocyanic
803 acid (HNCO), *Geophys. Res. Lett.*, **43**(8), 4033–4041, doi:10.1002/2016GL068207, 2016.

804 Lippmann, M.: Health effects of tropospheric ozone, *Environ. Sci. Technol.*, **25**(12), 1954–1962,
805 doi:10.1021/es00024a001, 1991.

806 Liu, P. F., Abdelmalki, N., Hung, H.-M., Wang, Y., Brune, W. H. and Martin, S. T.: Ultraviolet and visible
807 complex refractive indices of secondary organic material produced by photooxidation of the aromatic
808 compounds toluene and m-Xylene, *Atmos. Chem. Phys.*, **15**(3), 1435–1446, doi:10.5194/acp-15-1435-
809 2015, 2015.

810 Mao, J., Ren, X., Brune, W. H., Olson, J. R., Crawford, J. H., Fried, a., Huey, L. G., Cohen, R. C., Heikes, B.,
811 Singh, H. B., Blake, D. R., Sachse, G. W., Diskin, G. S., Hall, S. R. and Shetter, R. E.: Airborne measurement
812 of OH reactivity during INTEX-B, *Atmos. Chem. Phys.*, **9**(1), 163–173, doi:10.5194/acp-9-163-2009, 2009.

813 Martinsson, J., Eriksson, A. C., Nielsen, I. E., Malmberg, V. B., Ahlberg, E., Andersen, C., Lindgren, R.,
814 Nyström, R., Nordin, E. Z., Brune, W. H., Svenningsson, B., Swietlicki, E., Boman, C. and Pagels, J. H.:
815 Impacts of Combustion Conditions and Photochemical Processing on the Light Absorption of Biomass
816 Combustion Aerosol, *Environ. Sci. Technol.*, **49**(24), 14663–14671, doi:10.1021/acs.est.5b03205, 2015.

817 Matsunaga, A. and Ziemann, P. J.: Gas-Wall Partitioning of Organic Compounds in a Teflon Film Chamber
818 and Potential Effects on Reaction Product and Aerosol Yield Measurements, *Aerosol Sci. Technol.*, **44**(10),
819 881–892, doi:10.1080/02786826.2010.501044, 2010.

820 [Moise, T. and Rudich, Y.: Reactive Uptake of Ozone by Aerosol-Associated Unsaturated Fatty Acids:
821 Kinetics, Mechanism, and Products, *J. Phys. Chem. A*, **106**\(27\), 6469–6476, doi:10.1021/jp025597e,
822 2002.](#)

823 [Moise, T., Talukdar, R. K., Frost, G. J., Fox, R. W. and Rudich, Y.: Reactive uptake of NO3 by liquid and
824 frozen organics, *J. Geophys. Res.*, **107**\(D2\), 4014, doi:10.1029/2001JD000334, 2002.](#)

825 [Nehr, S., Bohn, B., Fuchs, H., Häseler, R., Hofzumahaus, A., Li, X., Rohrer, F., Tillmann, R. and Wahner, A.:
826 Atmospheric photochemistry of aromatic hydrocarbons: OH budgets during SAPHIR chamber
827 experiments, *Atmos. Chem. Phys.*, **14**\(13\), 6941–6952, doi:10.5194/acp-14-6941-2014, 2014.](#)

828 Nel, A.: Air Pollution-Related Illness: Effects of Particles, *Science* (80-.), **308**(5723), 804–806,
829 doi:10.1126/science.1108752, 2005.

830 Ng, N. L., Canagaratna, M. R., Zhang, Q., Jimenez, J. L., Tian, J., Ulbrich, I. M., Kroll, J. H., Docherty, K. S.,
831 Chhabra, P. S., Bahreini, R., Murphy, S. M., Seinfeld, J. H., Hildebrandt, L., Donahue, N. M., DeCarlo, P. F.,
832 Lanz, V. a., Prévôt, a. S. H., Dinar, E., Rudich, Y., Worsnop, D. R., Prevot, A. S. H., Dinar, E., Rudich, Y. and

Deleted: . Discuss., (January), 1–20

Deleted: 2016-394

835 Worsnop, D. R.: Organic aerosol components observed in Northern Hemispheric datasets from Aerosol
836 Mass Spectrometry, *Atmos. Chem. Phys.*, 10(10), 4625–4641, doi:10.5194/acp-10-4625-2010, 2010.

837 Odum, J. R., Hoffmann, T., Bowman, F., Collins, D., Flagan Richard, C. and Seinfeld John, H.: Gas particle
838 partitioning and secondary organic aerosol yields, *Environ. Sci. Technol.*, 30(8), 2580–2585,
839 doi:10.1021/es950943+, 1996.

840 Orlando, J. J. and Tyndall, G. S.: Laboratory studies of organic peroxy radical chemistry: an overview with
841 emphasis on recent issues of atmospheric significance, *Chem. Soc. Rev.*, 41(19), 6294,
842 doi:10.1039/c2cs35166h, 2012.

843 Ortega, A. M., Day, D. A., Cubison, M. J., Brune, W. H., Bon, D., de Gouw, J. A. and Jimenez, J. L.:
844 Secondary organic aerosol formation and primary organic aerosol oxidation from biomass-burning
845 smoke in a flow reactor during FLAME-3, *Atmos. Chem. Phys.*, 13(22), 11551–11571, doi:10.5194/acp-
846 13-11551-2013, 2013.

847 Ortega, A. M., Hayes, P. L., Peng, Z., Palm, B. B., Hu, W., Day, D. A., Li, R., Cubison, M. J., Brune, W. H.,
848 Graus, M., Warneke, C., Gilman, J. B., Kuster, W. C., de Gouw, J., Gutiérrez-Montes, C. and Jimenez, J. L.:
849 Real-time measurements of secondary organic aerosol formation and aging from ambient air in an
850 oxidation flow reactor in the Los Angeles area, *Atmos. Chem. Phys.*, 16(11), 7411–7433,
851 doi:10.5194/acp-16-7411-2016, 2016.

852 Palm, B. B., Campuzano-Jost, P., Day, D. A., Ortega, A. M., Fry, J. L., Brown, S. S., Zarzana, K. J., Dube, W.,
853 Wagner, N. L., Draper, D. C., Kaser, L., Jud, W., Karl, T., Hansel, A., Gutiérrez-Montes, C. and Jimenez, J.
854 L.: Secondary organic aerosol formation from in situ OH, O₃, and NO₃ oxidation of ambient forest air in
855 an oxidation flow reactor, *Atmos. Chem. Phys.*, 17(8), 5331–5354, doi:10.5194/acp-17-5331-2017, 2017.

856 Palm, B. B., Campuzano-Jost, P., Ortega, A. M., Day, D. A., Kaser, L., Jud, W., Karl, T., Hansel, A., Hunter, J.
857 F., Cross, E. S., Kroll, J. H., Peng, Z., Brune, W. H. and Jimenez, J. L.: In situ secondary organic aerosol
858 formation from ambient pine forest air using an oxidation flow reactor, *Atmos. Chem. Phys.*, 16(5),
859 2943–2970, doi:10.5194/acp-16-2943-2016, 2016.

860 Peng, Z., Carrasco, N. and Pernot, P.: Modeling of synchrotron-based laboratory simulations of Titan's
861 ionospheric photochemistry, *GeoResJ*, 1–2, 33–53, doi:10.1016/j.grj.2014.03.002, 2014.

862 Peng, Z., Day, D. A., Ortega, A. M., Palm, B. B., Hu, W., Stark, H., Li, R., Tsigaridis, K., Brune, W. H. and
863 Jimenez, J. L.: Non-OH chemistry in oxidation flow reactors for the study of atmospheric chemistry
864 systematically examined by modeling, *Atmos. Chem. Phys.*, 16(7), 4283–4305, doi:10.5194/acp-16-
865 4283-2016, 2016.

866 Peng, Z., Day, D. A., Stark, H., Li, R., Lee-Taylor, J., Palm, B. B., Brune, W. H. and Jimenez, J. L.: HOx radical
867 chemistry in oxidation flow reactors with low-pressure mercury lamps systematically examined by
868 modeling, *Atmos. Meas. Tech.*, 8(11), 4863–4890, doi:10.5194/amt-8-4863-2015, 2015.

869 Ranney, A. P. and Ziemann, P. J.: Kinetics of Acid-Catalyzed Dehydration of Cyclic Hemiacetals in Organic
870 Aerosol Particles in Equilibrium with Nitric Acid Vapor, *J. Phys. Chem. A*, 120(16), 2561–2568,
871 doi:10.1021/acs.jpca.6b01402, 2016.

872 Richards-Henderson, N. K., Goldstein, A. H. and Wilson, K. R.: Large Enhancement in the Heterogeneous
873 Oxidation Rate of Organic Aerosols by Hydroxyl Radicals in the Presence of Nitric Oxide, *J. Phys. Chem.*
874 *Lett.*, 6, 4451–4455, doi:10.1021/acs.jpcl.5b02121, 2015.

875 Saltelli, A., Ratto, M., Tarantola, S. and Campolongo, F.: Sensitivity Analysis for Chemical Models, *Chem.*
876 *Rev.*, 105(7), 2811–2828, doi:10.1021/cr040659d, 2005.

877 Sander, S. P., Friedl, R. R., Barker, J. R., Golden, D. M., Kurylo, M. J., Wine, P. H., Abbatt, J. P. D., Burkholder,
878 J. B., Kolb, C. E., Moortgat, G. K., Huie, R. E. and Orkin, V. L.: Chemical Kinetics and Photochemical Data
879 for Use in Atmospheric Studies Evaluation Number 17, Pasadena, CA, USA. [online] Available from:
880 http://jpldataeval.jpl.nasa.gov/pdf/JPL_10-6_Final_15June2011.pdf, 2011.

881 Schill, G. P., Jathar, S. H., Kodros, J. K., Levin, E. J. T., Galang, A. M., Friedman, B., Link, M. F., Farmer, D.
882 K., Pierce, J. R., Kreidenweis, S. M. and DeMott, P. J.: Ice-nucleating particle emissions from
883 photochemically aged diesel and biodiesel exhaust, *Geophys. Res. Lett.*, 43(10), 5524–5531,
884 doi:10.1002/2016GL069529, 2016.

885 Schwantes, R. H., Schilling, K. A., McVay, R. C., Lignell, H., Coggon, M. M., Zhang, X., Wennberg, P. O. and

Deleted: O&sub>3&sub>

Deleted: NO&sub>3&sub>

Deleted: . Discuss., 1–46

Deleted: 2016-1080

890 [Seinfeld, J. H.: Formation of highly oxygenated low-volatility products from cresol oxidation, Atmos.](#)
891 [Chem. Phys., 17\(5\), 3453–3474, doi:10.5194/acp-17-3453-2017, 2017.](#)

892 Seakins, P. W.: A brief review of the use of environmental chambers for gas phase studies of kinetics,
893 chemical mechanisms and characterisation of field instruments, EPJ Web Conf., 9, 143–163,
894 doi:10.1051/epjconf/201009012, 2010.

895 Simonen, P., Saukko, E., Karjalainen, P., Timonen, H., Bloss, M., Aakko-Saksa, P., Rönkkö, T., Keskinen, J.
896 and Dal Maso, M.: A [new oxidation flow reactor for measuring secondary aerosol formation of rapidly](#)
897 [changing emission sources](#), Atmos. Meas. Tech., [10\(4\), 1519–1537](#), doi:10.5194/amt-10-1519-2017,
898 [2017](#).

899 Stocker, T. F., Qin, D., Plattner, G.-K., Tignor, M., Allen, S. K., Boschung, J., Nauels, A., Xia, Y., Bex, V. and
900 Midgley, P. M.: Climate Change 2013 - The Physical Science Basis, edited by Intergovernmental Panel on
901 Climate Change, Cambridge University Press, Cambridge., 2014.

902 Strollo, C. M. and Ziemann, P. J.: Products and mechanism of secondary organic aerosol formation from
903 the reaction of 3-methylfuran with OH radicals in the presence of NO_x, Atmos. Environ., 77, 534–543,
904 doi:10.1016/j.atmosenv.2013.05.033, 2013.

905 Tkacik, D. S., Lambe, A. T., Jathar, S., Li, X., Presto, A. A., Zhao, Y., Blake, D., Meinardi, S., Jayne, J. T.,
906 Croteau, P. L. and Robinson, A. L.: Secondary Organic Aerosol Formation from in-Use Motor Vehicle
907 Emissions Using a Potential Aerosol Mass Reactor, Environ. Sci. Technol., 48(19), 11235–11242,
908 doi:10.1021/es502239v, 2014.

909 Volkamer, R., Jimenez, J. L., San Martini, F., Dzepina, K., Zhang, Q., Salcedo, D., Molina, L. T., Worsnop,
910 D. R. and Molina, M. J.: Secondary organic aerosol formation from anthropogenic air pollution: Rapid
911 and higher than expected, Geophys. Res. Lett., 33(17), L17811, doi:10.1029/2006GL026899, 2006.

912 Wang, J., Doussin, J. F., Perrier, S., Perraudin, E., Katrib, Y., Pangu, E. and Picquet-Varrault, B.: Design of
913 a new multi-phase experimental simulation chamber for atmospheric photochemistry, aerosol and cloud
914 chemistry research, Atmos. Meas. Tech., 4(11), 2465–2494, doi:10.5194/amt-4-2465-2011, 2011.

915 Zhang, X., Cappa, C. D., Jathar, S. H., McVay, R. C., Ensberg, J. J., Kleeman, M. J. and Seinfeld, J. H.:
916 Influence of vapor wall loss in laboratory chambers on yields of secondary organic aerosol., Proc. Natl.
917 Acad. Sci. U. S. A., 111(16), 5802–7, doi:10.1073/pnas.1404727111, 2014.

918 Ziemann, P. [J.](#) and Atkinson, R.: Kinetics, products, and mechanisms of secondary organic aerosol
919 formation, Chem. Soc. Rev., 41(19), 6582, doi:10.1039/c2cs35122f, 2012.

920

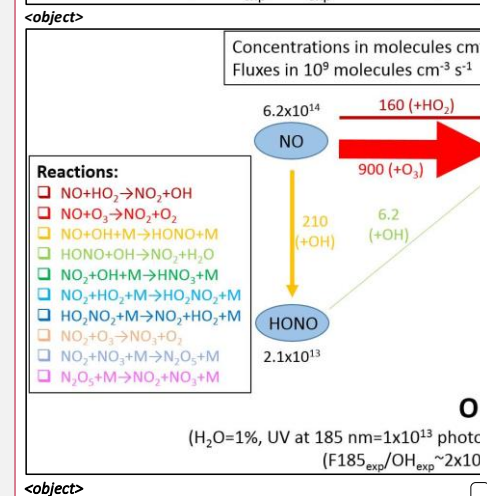
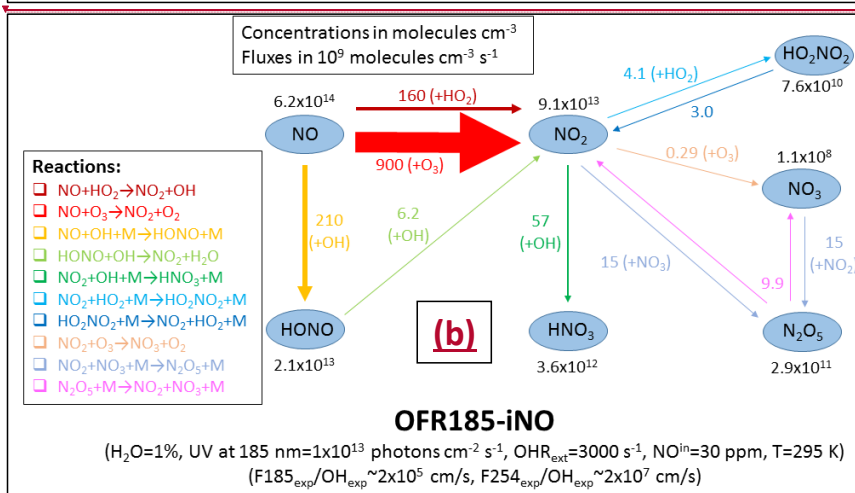
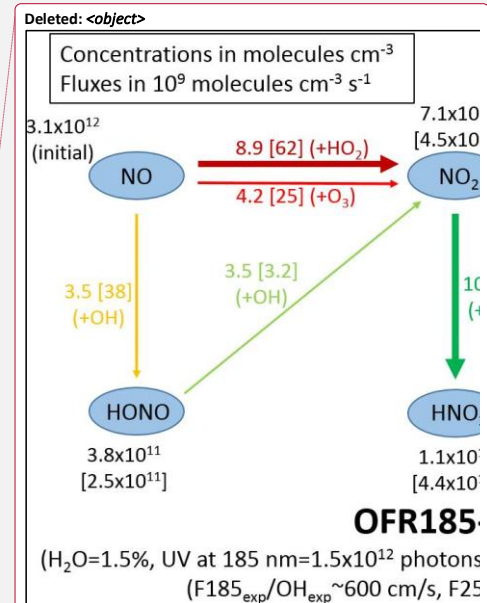
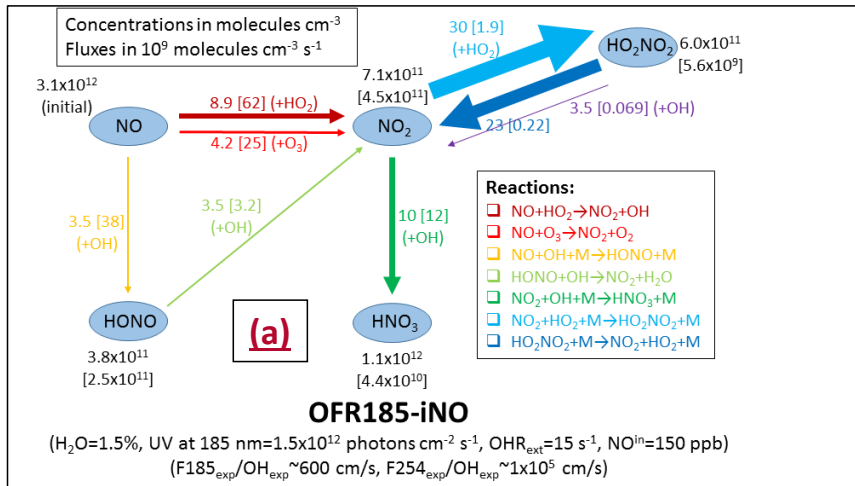
Deleted: New Oxidation Flow Reactor

Deleted: Measuring Secondary Aerosol Formation

Deleted: Rapidly Changing Emission Sources

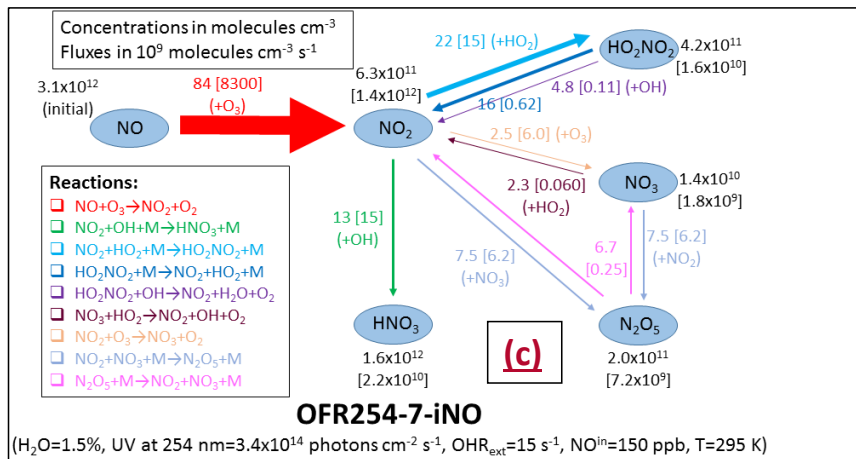
Deleted: . Discuss., (November), 1–27

Deleted: 2016-300, 2016



926

927



939

940

941

942

943

944

945

946

947

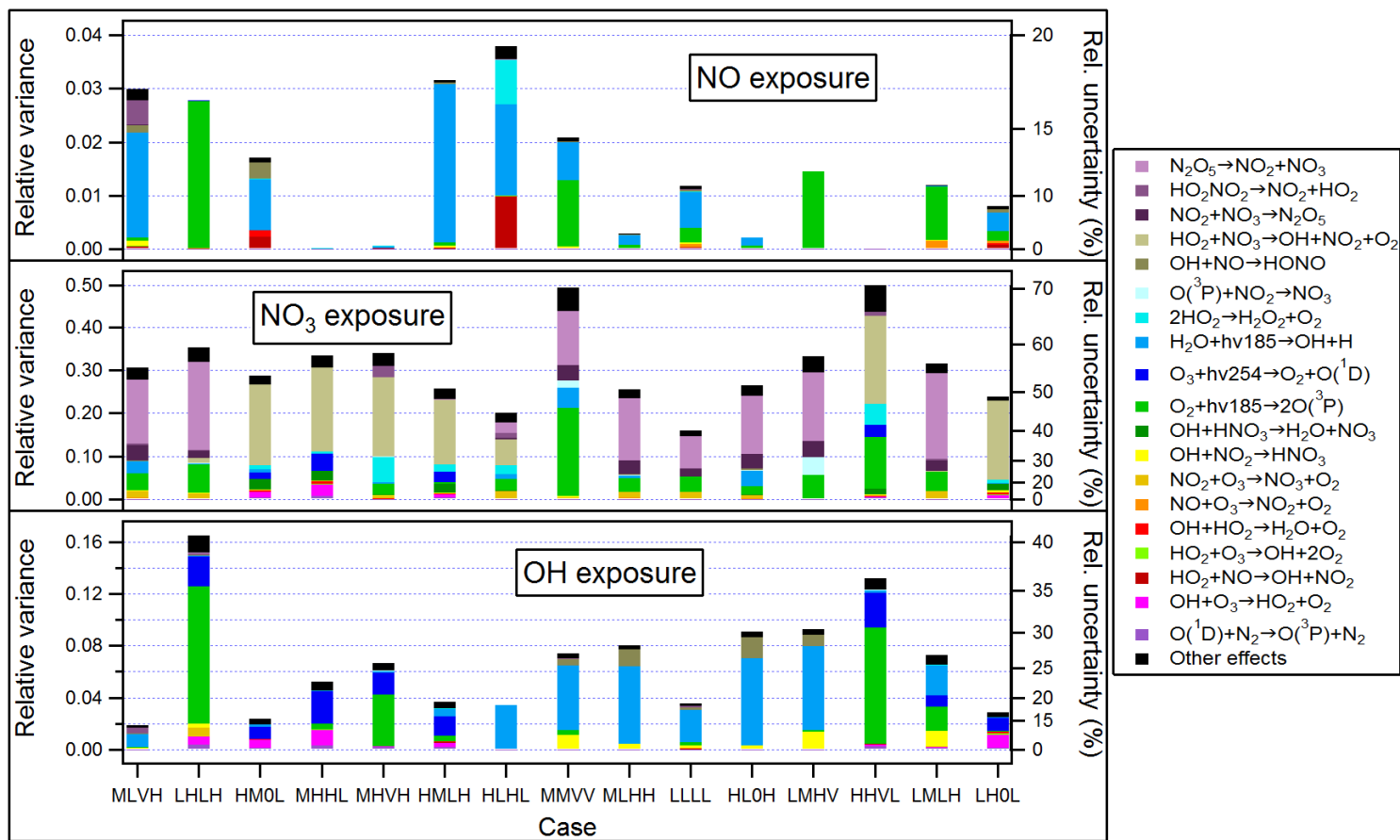
948

949

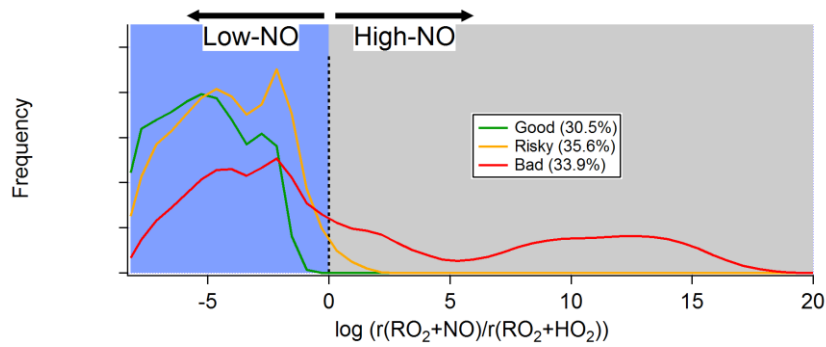
950

951

Figure 1. Schematics of main N-containing species and their major interconversion pathways under typical input conditions for (a) OFR185-iNO with NOⁱⁿ=150 ppb, (b) OFR254-7-iNO with NOⁱⁿ=150 ppb, and (c) OFR185-iNO with NOⁱⁿ=30 ppm. Species average concentrations (in molecules cm⁻³) are shown in black beside species names. Arrows denote directions of the conversions. Average reaction fluxes (in units of 10⁹ molecules cm⁻³ s⁻¹) are calculated according to the production rate, and shown on or beside the corresponding arrows and in the same color. Within each schematic, the thickness of the arrows is a measure of their corresponding species flux. Multiple arrows in the same color and pointing to the same species should be counted only once for reaction flux on a species. Note that all values in these schematics are average ones over the residence time, except for those in square brackets in panels a and b, which are average values within approximate NO effective lifetime (τ_{NO} , or more accurately, an integer multiple of the model's output time step closest to NO effective lifetime). All concentrations and fluxes have two significant digits.



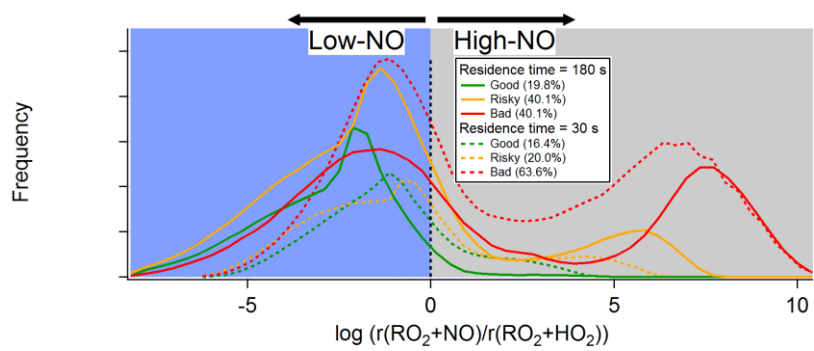
953 **Figure 2.** Relative variances (left axes)/uncertainties (right axes) of several outputs (i.e., NO, NO₃, and OH exposures) of Monte Carlo uncertainty propagation, and relative
954 contributions of key reactions to these relative variances in several typical cases (denoted in 4-character labels, see Table 2 for the typical case label code) in OFR185-iNO.
955 Relative variances are shown in linear scales (left axis), while corresponding relative uncertainties, equal to relative variances' square roots, are indicated by the non-linear
956 right axis. Only the reactions with a contribution of no less than 0.04 to at least one relative variance are shown.



957

958

(a) OFR254-iNO



959

960

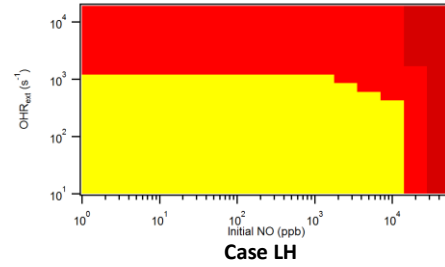
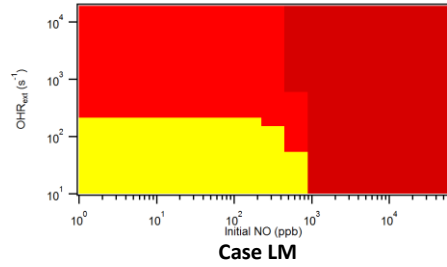
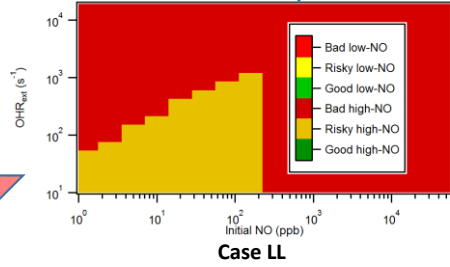
(b) OFR185-iNO

961 **Figure 3.** Frequency occurrence distributions of good, risky, and bad conditions (see Table 3) over
 962 logarithm of the ratio between RO_2 reacted with NO and with HO_2 (see Section S1 for more detail) for
 963 (a) OFR254-iNO (only the case with a residence time of 180 s) and (b) OFR185-iNO (including two cases
 964 with residence times of 180 and 30 s). Low and high-NO regions (see Table 3) are colored in light blue
 965 and grey, respectively.

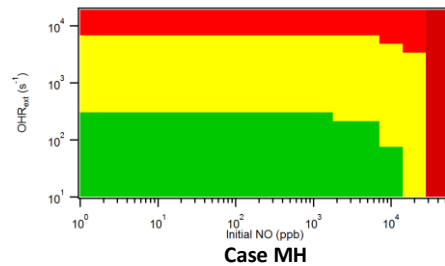
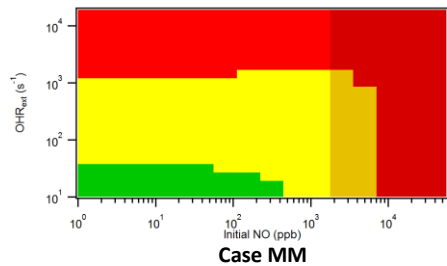
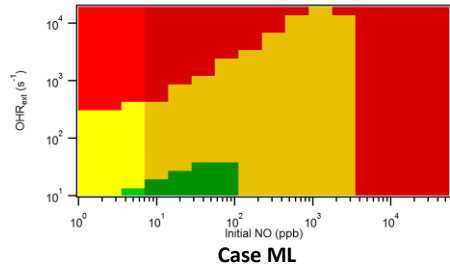
966
967

Increasing UV

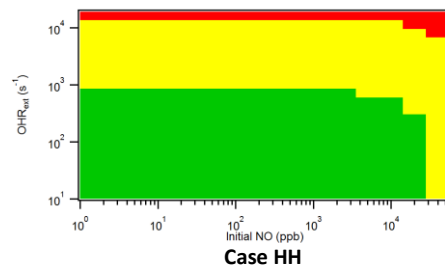
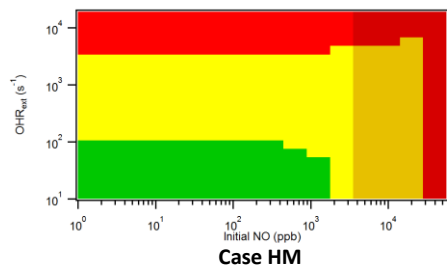
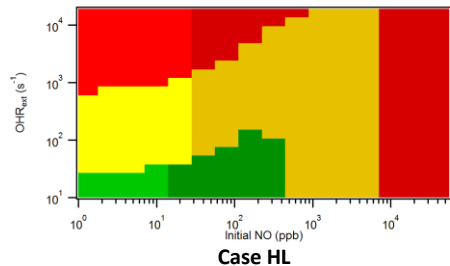
Increasing H₂O



968
969



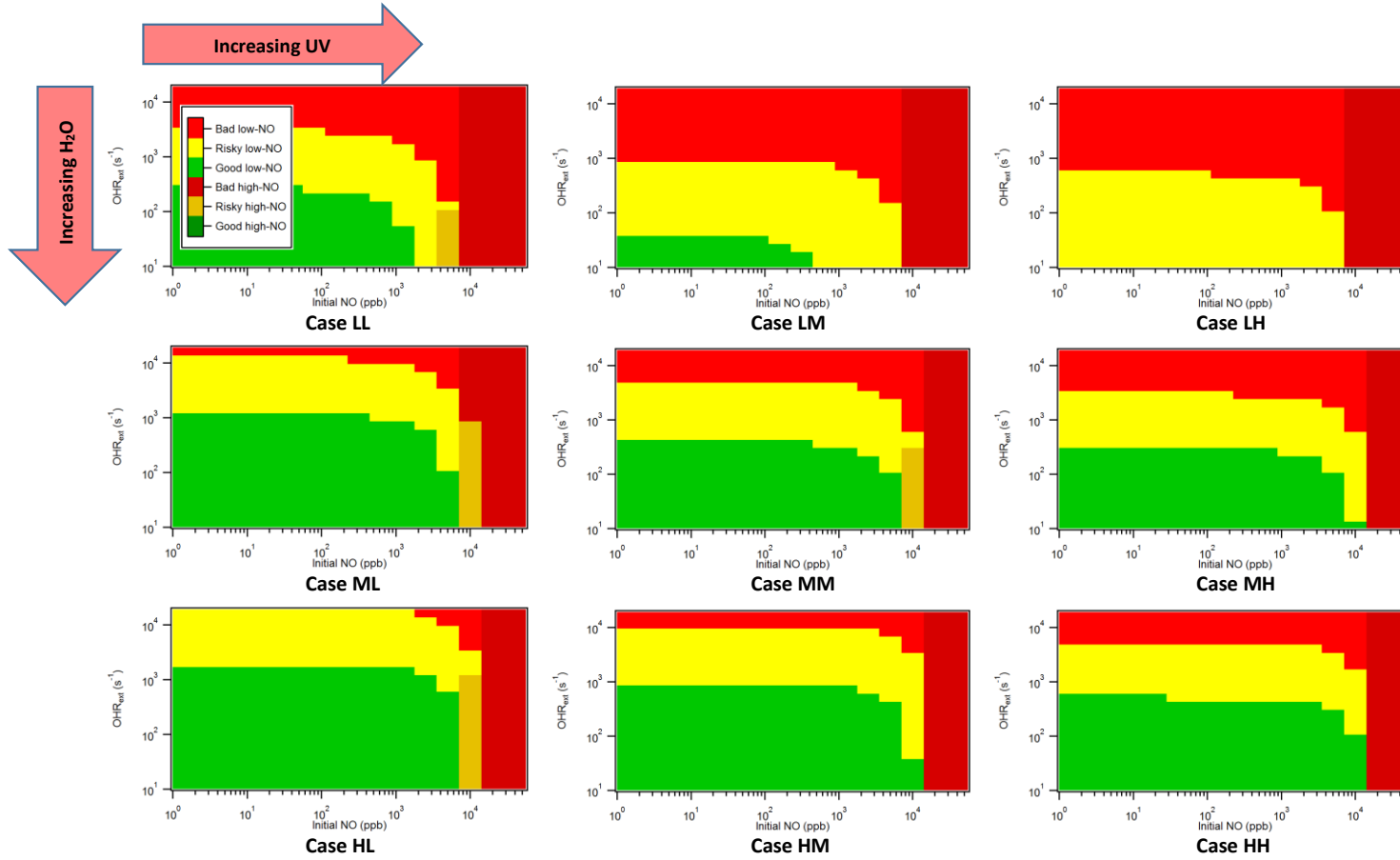
970
971



972
973

974 **Figure 4.** Image plots of the condition types defined in Table 3 vs. external OH reactivity (excluding N-containing species) and initial NO for several typical cases in OFR185-
975 iNO (see Table 2 for the case label code).
976

977
978

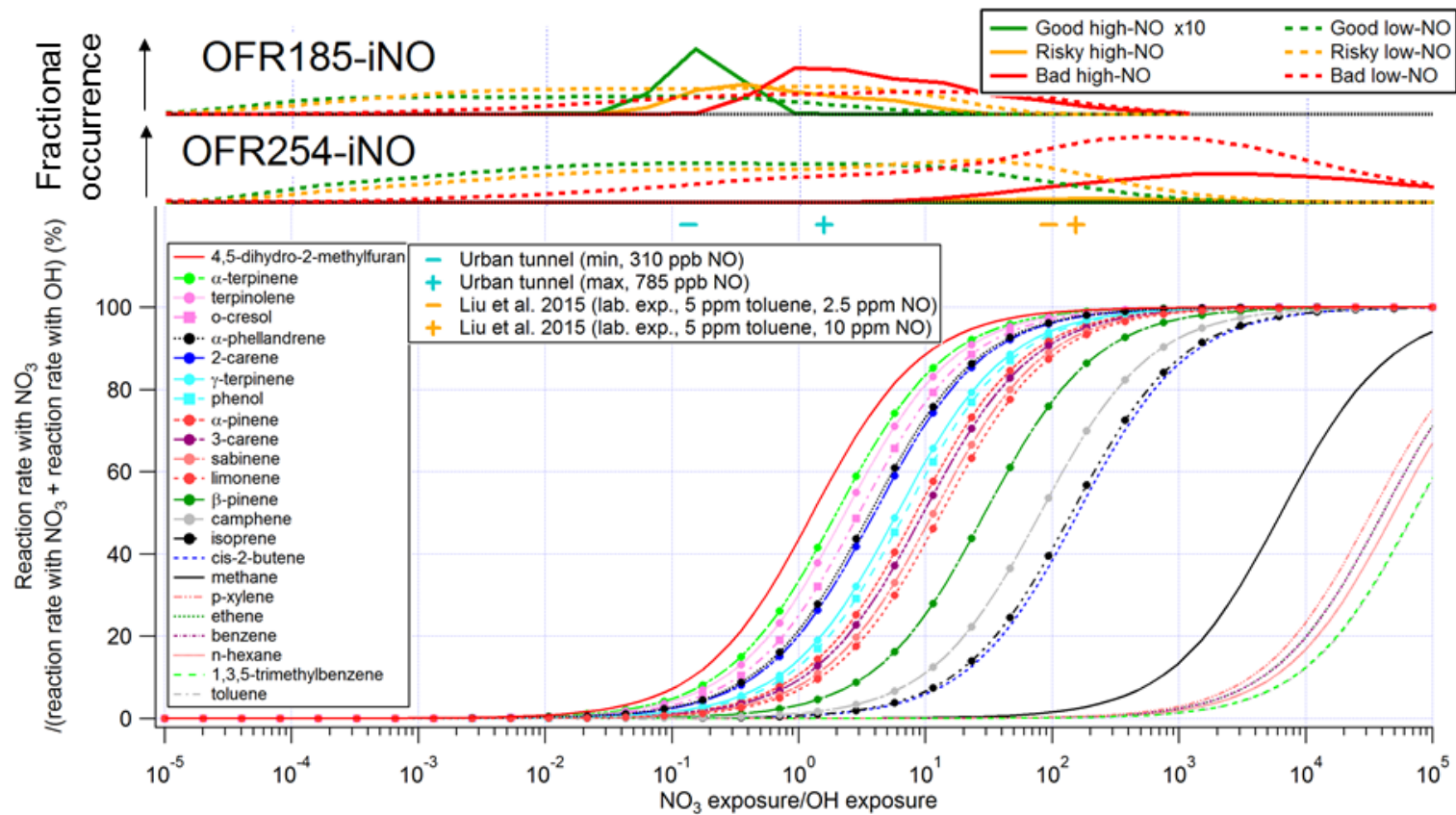


979
980

981
982

983
984

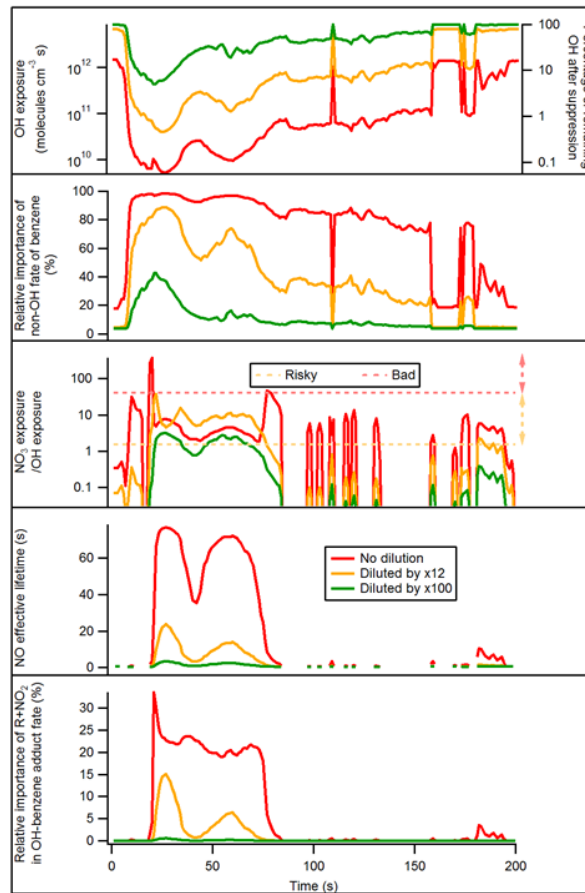
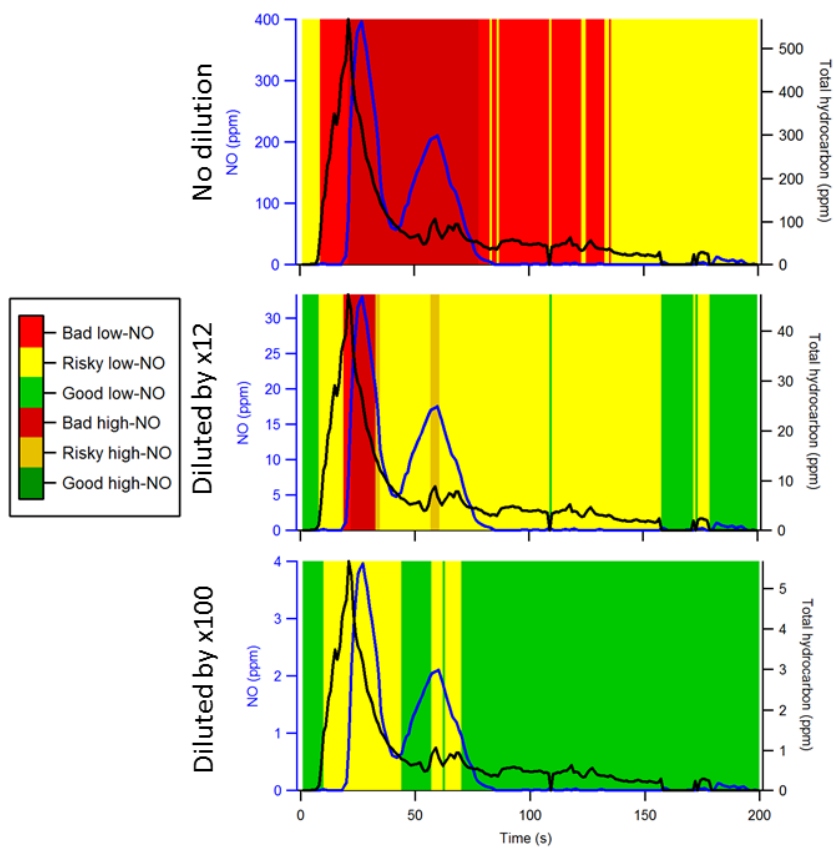
985 **Figure 5.** Same format as Fig. 4, but for OFR254-22-INO.



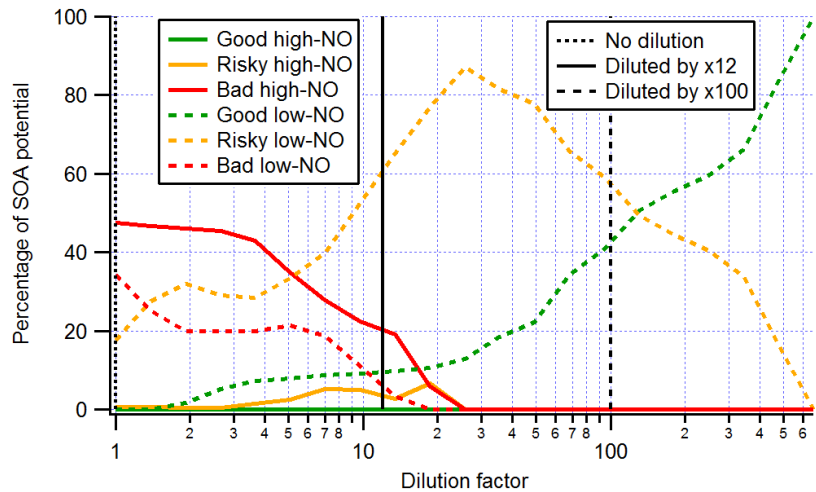
986
987
988

Figure 6. Fractional importance of the reaction rate of several species of interest with NO_3 vs. that with OH, as a function of the ratio of exposure to NO_3 and OH. The curves of biogenics and phenols are highlighted by solid dots and squares, respectively. The turquoise and orange markers show the ranges of modeled exposure ratios between NO_3

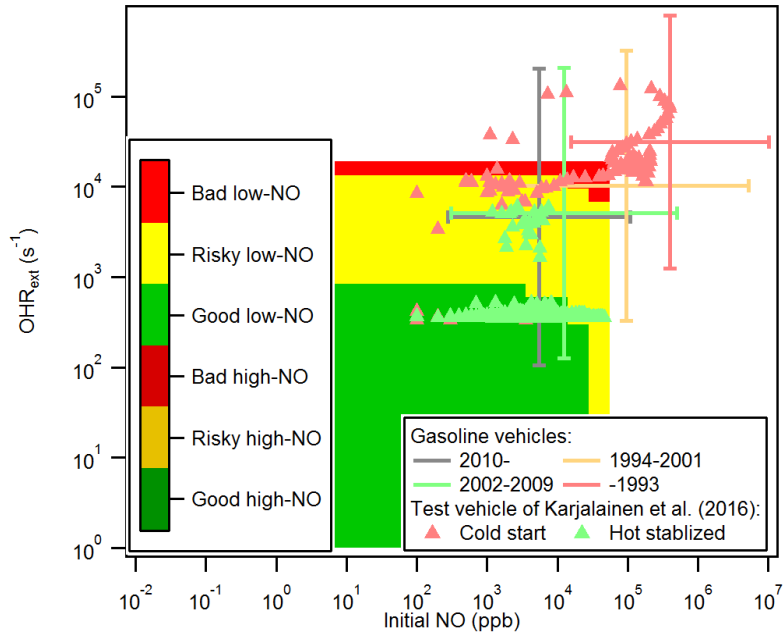
989 and OH of a source study in an urban tunnel (Tkacik et al., 2014) and a laboratory study (Liu et al., 2015) using OFR, respectively. In the upper part of the figure, the modeled
990 frequency distributions of ratios of NO₃ exposure to OH exposure under good/risky/bad high/low-NO conditions for OFR185-iNO and OFR254-iNO are also shown. See Table
991 3 for the definitions of the three types of conditions. All curves, markers, and histograms in this figure share the same abscissa.
992



994 **Figure 7.** (left) NO and total hydrocarbon during the first 200 s of the test of Karjalainen et al. (2016) in the cases of no dilution, dilution by a factor of 12 (as actually done in
995 that study), and dilution by a factor of 100. Different periods of time are colored according to corresponding emissions (i.e., input conditions for OFR), classified as
996 good/risky/bad high/low-NO. (right) OH exposure/percentage of remaining OH after suppression, relative importance of non-OH fate of benzene, exposure ratio of NO₃ to
997 OH, NO effective lifetime, and relative importance of reaction of OH-toluene adduct with NO₂ in the fate of this adduct in the OFR of Karjalainen et al. (2016) during the first
998 200 s of their test in the cases of no dilution, dilution by a factor of 12, and dilution by a factor of 100. Horizontal orange and red dashed lines in the middle right panel denote
999 “risky” and “bad” regions for exposure ratio of NO₃ to OH, respectively. Above the orange (red) dashed line, reaction with NO₃ contributes >20% to the fate of phenol (isoprene).



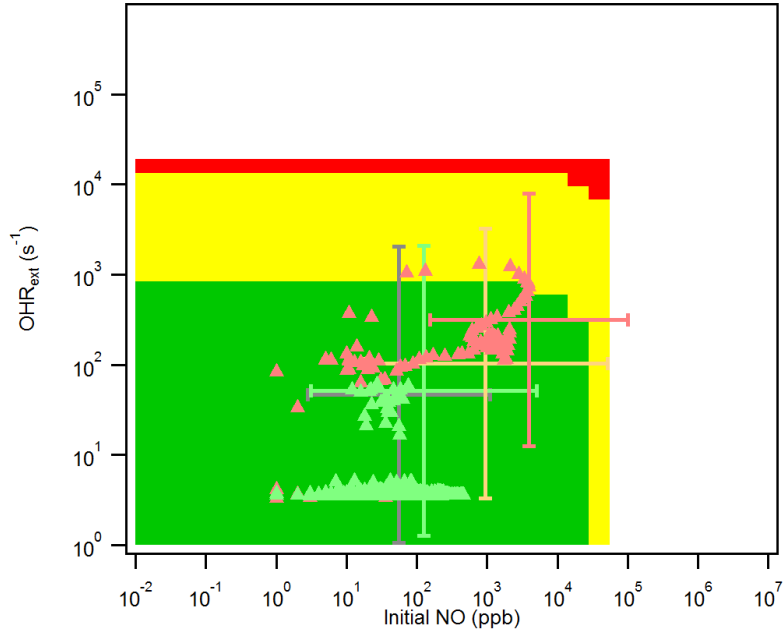
1000
 1001 **Figure 8.** Secondary organic aerosol (SOA) potential (estimated from the total hydrocarbon
 1002 measurement) in the OFR of Karjalainen et al. (2016) formed during periods of time in the OFR
 1003 corresponding to good/risky/bad high/low-NO conditions, as a function of dilution factor. Vertical lines
 1004 denoting dilution factors of 1, 12 (as actually used in that study), and 100 are also shown.
 1005



1006

1007

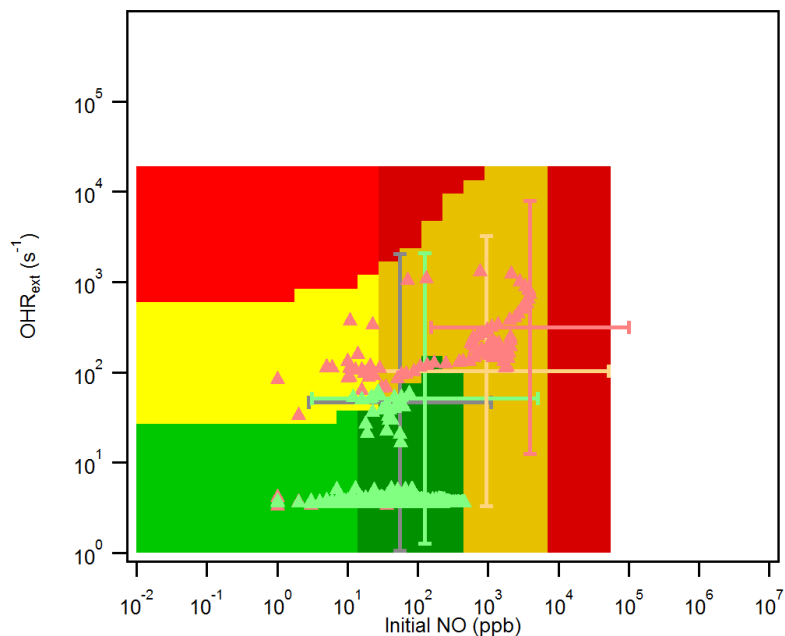
(a) No dilution (background: Case HH)



1008

1009

(b) Dilution by a factor of 100 (background: Case HH)



(c) Dilution by a factor of 100 (background: Case HL)

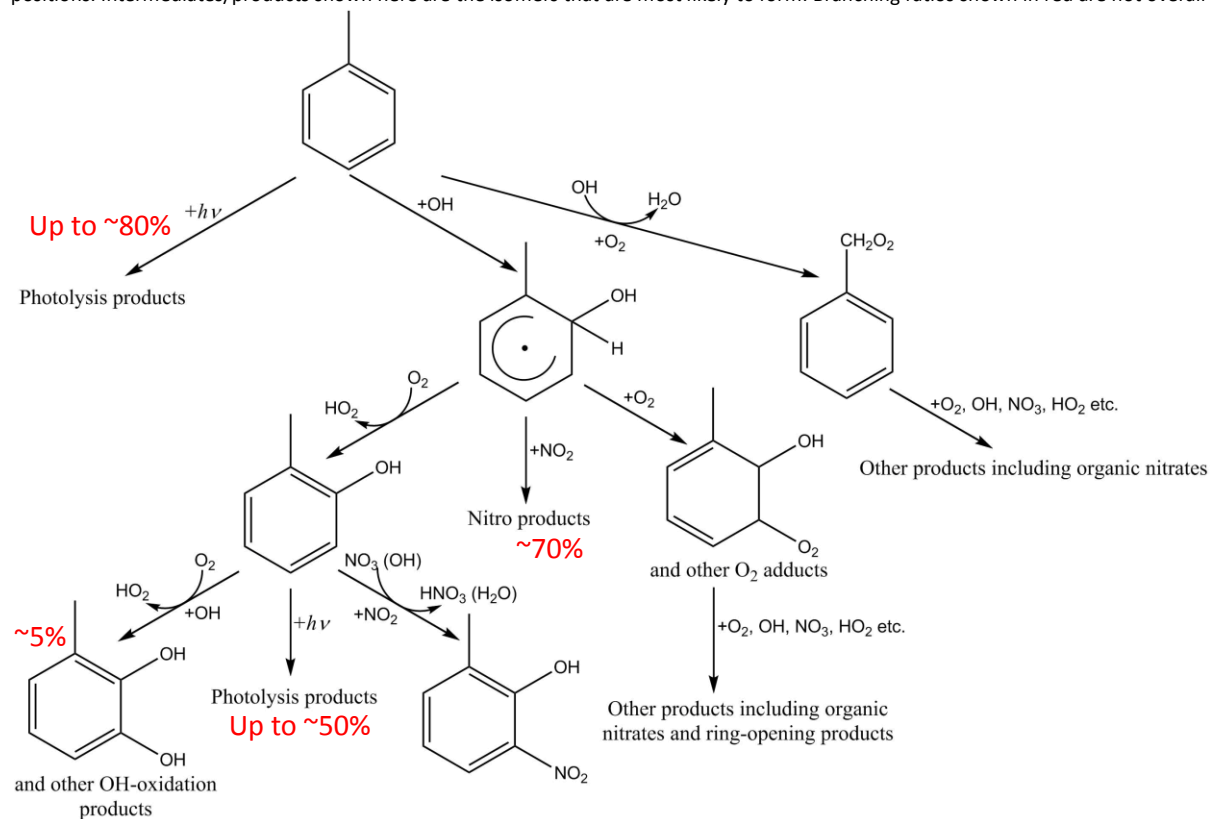
1010

1011

1012 **Figure 9.** Location of individual 1 s datapoints vs. OFR185-iNO reaction conditions. Datapoints are shown
 1013 from the test vehicle of Karjalainen et al. (2016), as well as average exhaust from gasoline vehicle on-
 1014 road emissions measured by Bishop and Stedman (2013). On-road emissions are classified by vehicle
 1015 year and the distribution of each category is shown as a cross representing 1 standard deviation (with
 1016 log-normal distribution assumed). The X and Y axes are NO and external OH reactivity (excluding N-
 1017 containing species) due to vehicle emissions in OFR in the cases of (a) no dilution and (b,c) dilution by a
 1018 factor of 100. The Karjalainen et al. (2016) points are classified as cold start (during first 200 s) and hot
 1019 stabilized (during 200–1000 s). In addition, the same image plots as the panels of Cases HH (high H₂O
 1020 and high UV, see Table 2 for the case label code) and HL in Fig. 4 (OFR185-iNO) are shown as background
 1021 for comparison.

1022

1023 **Scheme 1.** Possible major reactions in an OFR254-13-iNO with 5 ppm toluene and 10 ppm initial NO. Branching ratios in red are estimated by the model and/or according to
 1024 Calvert et al. (2002), Atkinson and Arey (2003), Ziemann and Atkinson (2012), and Peng et al. (2016). Note that addition/substitution on the aromatic ring may occur at other
 1025 positions. Intermediates/products shown here are the isomers that are most likely to form. Branching ratios shown in red are not overall but from immediate reactant.



1026

1027

Table 1. Experimental conditions of several OFR studies with high NO injection.

Study	Source type	Temperature (K)	Relative humidity (%)	Dilution factor	External OH reactivity of undiluted source (s ⁻¹)	Source NO _x concentration (ppm)
Link et al. (2016)	Diesel vehicle emission		50	45–110	~5000 ^{*1}	436 ^{*1}
Martinsson et al. (2015)	Biomass burning emission			1700	156400 ^{*1}	154
Karjalainen et al. (2016)	Gasoline vehicle emission	295	60	12	~73000 ^{*2,a}	~400 ^{*1,b}
Liu et al. (2015)	Purified gas	293	13	1	~1400 ^{*1,a}	10 ^{*1,b}
Tkacik et al. (2014)	Tunnel air	293	42	1	~60 ^{*1,a}	~0.8 ^{*1}
Ortega et al. (2013)	Biomass burning emission	290	30	~500	~15-500	~0.2

^{*1} maximum value in the study^{*2} value at the moment of maximum NO emission^{*a} NO_y species excluded^{*b} NO only1028
1029
1030
1031
1032

1033 **Table 2.** Code of the labels of typical cases. A case label can be composed of four characters denoting the water mixing ratio, the photon flux, the external OH reactivity
 1034 excluding N-containing species, and the initial NO mixing ratio, respectively. A case label can also be composed of two characters denoting the water mixing ratio and the
 1035 photon flux.

	Water mixing ratio	Photon flux	External OH reactivity (no ON)	Initial NO mixing ratio
	L=low (0.07%)	L=low (10^{11} photons $\text{cm}^{-2} \text{s}^{-1}$ at 185 nm; 4.2×10^{13} photons $\text{cm}^{-2} \text{s}^{-1}$ at 254 nm)	0	0
Options	M=medium (1%)	M=medium (10^{13} photons $\text{cm}^{-2} \text{s}^{-1}$ at 185 nm; 1.4×10^{15} photons $\text{cm}^{-2} \text{s}^{-1}$ at 254 nm)	L=low (10 s^{-1})	L=low (10 ppb)
	H=high (2.3%)	H=high (10^{14} photons $\text{cm}^{-2} \text{s}^{-1}$ at 185 nm; 8.5×10^{15} photons $\text{cm}^{-2} \text{s}^{-1}$ at 254 nm)	H=high (100 s^{-1})	H=high (316 ppb)
			V=very high (1000 s^{-1})	V=very high (10 ppm)
Example	LHOV:	low water mixing ratio, high photon flux, no external OH reactivity (excluding ON), very high initial NO mixing ratio		
	ML:	medium water mixing ratio, low photon flux		

1036
1037

1038 **Table 3.** Definition of condition types in this study (good/risky/bad high/low-NO).

Condition	Good	Risky	Bad
Criterion	$F_{185_{\text{exp}}}/OH_{\text{exp}} < 3 \times 10^3 \text{ cm s}^{-1}$ and $F_{254_{\text{exp}}}/OH_{\text{exp}} < 4 \times 10^5 \text{ cm s}^{-1}$	$F_{185_{\text{exp}}}/OH_{\text{exp}} < 1 \times 10^5 \text{ cm s}^{-1}$ and $F_{254_{\text{exp}}}/OH_{\text{exp}} < 1 \times 10^7 \text{ cm s}^{-1}$ (excluding good conditions)	$F_{185_{\text{exp}}}/OH_{\text{exp}} \geq 1 \times 10^5 \text{ cm s}^{-1}$ or $F_{254_{\text{exp}}}/OH_{\text{exp}} \geq 1 \times 10^7 \text{ cm s}^{-1}$
Condition	High-NO	Low-NO	
Criterion*	$\frac{r(\text{RO}_2 + \text{NO})}{r(\text{RO}_2 + \text{HO}_2)} > 1$	$\frac{r(\text{RO}_2 + \text{NO})}{r(\text{RO}_2 + \text{HO}_2)} \leq 1$	

* See Section S1 for detail.

1039
1040

1041
1042
1043

Table 4. Statistics of the ratio between OH exposures calculated in the model with the Lambe et al. (2011) residence time distribution ($OH_{exp,RTD}$) and in the plug-flow model ($OH_{exp,PF}$). The geometric mean, uncertainty factor (geometric standard deviation), and percentage of outlier cases (>3 or $<1/3$) are shown for OFR185-iNO, OFR254-70-iNO, and OFR254-7-iNO.

	<u>Geometric mean</u>	<u>Uncertainty factor</u>	<u>Outlier cases (%)</u>
<u>OFR185-iNO</u>	<u>1.91</u>	<u>1.64</u>	<u>11</u>
<u>OFR254-7-iNO</u>	<u>1.59</u>	<u>1.51</u>	<u>7</u>
<u>OFR254-70-iNO</u>	<u>1.48</u>	<u>1.29</u>	<u>3</u>

1044